Bearing Capacity of Deep Foundations in Sand

ALEKSANDAR B. VESIĆ, Associate Professor of Civil Engineering, Georgia Institute of Technology Soil Mechanics Laboratory

Large-scale model experiments have been made to provide information on factors which influence bearing capacity of deep foundations in sand. Cylindrical and prismatical foundations of various sizes resting at different depths in homogeneous sand masses of different relative densities were loaded statically to failure. Special loading cells permitted separate registration of point and skin loads throughout the tests. Additional tests with models of sand colored in layers were made to study the mechanism of shear failure in the soil mass. The model experiments were accompanied by standard laboratory tests for determination of physical characteristics of the soils used.

An analysis of shear patterns observed indicates that, depending on relative density of sand, all three types of failure previously described in the literature may occur at shallow depths: general shear failure, local shear failure and punching shear failure. However, at greater depths only punching shear failure occurs, irrespective of the relative density of sand.

The unit point and skin resistances of the foundation increase linearly with depth only at shallow depths. At greater depths, both resistances show a hyperbolic increase and reach asymptotically constant final values. These final values are independent of overburden pressure and appear to be functions of relative density of sand only. This is explained by the "arching" of sand above the foundation base.

Analyses of observed ultimate loads indicate that a fair estimate of bearing capacity can be made by assuming failure surfaces in accordance with observed shear patterns.

•FROM the point of view of soil mechanics, there are two general types of deep foundations. The first type may be represented by a foundation installed by some process of excavation or drilling which does not induce significant changes in density or structure of the bearing soil. Practically all piers and caissons and some piles belong to this type. The other type may be represented by a deep foundation forced into the ground by driving or a similar operation, that induces significant changes in adjacent soil. Most piles belong to this second type.

SCOPE

The present paper is an investigation of ultimate bearing capacity of deep foundations in homogeneous masses of sand. This problem is considered to be fundamental. Only after a thorough understanding of principles of behavior of deep foundations in homogeneous masses of soil will it be possible properly to see and treat the problems of different types of deep foundations encountered in engineering practice.

Paper sponsored by Committee on Stress Distribution in Earth Masses.

Theoretical Considerations

The basic problem of bearing capacity of deep foundations in sand can be formulated as follows: A rigid foundation of known shape and dimensions is placed at a depth D in a homogeneous mass of sand of defined physical properties (Fig. 1). A static, vertical, central load is applied on the top. What is the ultimate load Q that this foundation can support?

The load is generally transmitted partially along the foundation shaft or skin, partially at the foundation base or point. The two bearing components of the load, the skin load Q_s and the base or point load Q_p are usually considered separately. The total ultimate load is then expressed as the sum of these two components:

$$Q = Q_p + Q_s = p_o A_p + s_o A_s \qquad (1)$$

Here p_o represents the unit base resistance and s_o unit skin resistance of the foundation (psi or kg/cm^2). A_p and A_s are, respectively, bearing areas of the base and the skin.

The solution of the problem of bearing capacity of the base has been sought in the past primarily by an approach base on the classical work by Prandtl (1, 2), and Reissner (3). They presented a solution of the problem of penetration of a rigid stamp into an incompressible (rigid-plastic) solid (Fig. 2). That solution, first applied to the problem of bearing capacity of soils by Caquot (4) and Buisman (5) is usually written in the following general form (6):

$$p_o = c\, N_c\, \zeta_c + q\, N_q\, \zeta_q + \tfrac{1}{2}\, \gamma\, B\, N_\gamma\, \zeta_\gamma \qquad (2)$$

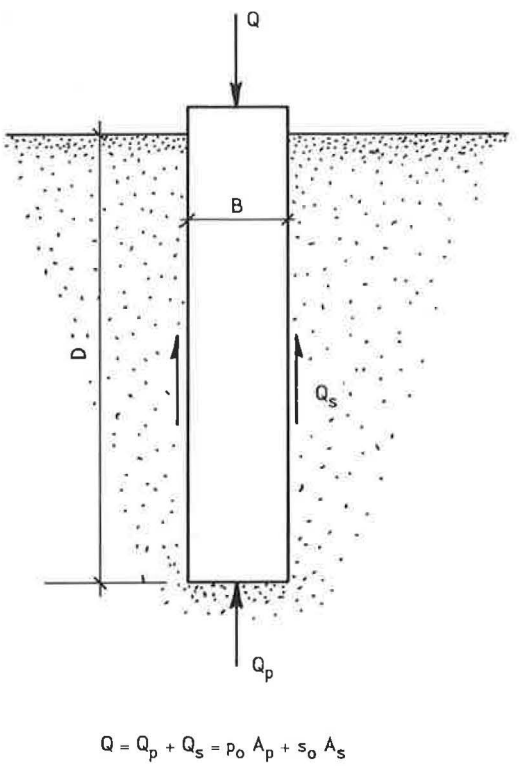

Figure 1. Basic problem of bearing capacity of a deep foundation.

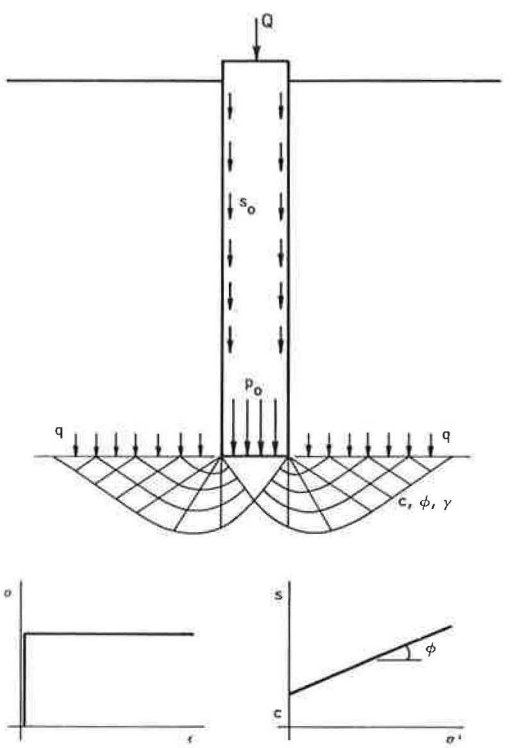

Figure 2. Prandtl-Reissner solution as applied by Caquot and Buisman.

In Eq. 2, c represents the shear strength intercept (cohesion) of the soil, q the overburden pressure, γ the unit weight of the soil involved in shear and B the foundation width. N_c, N_q, N_γ are bearing capacity factors for a strip foundation and ζ_c, ζ_q, ζ_γ are shape factors. Both N and ζ factors are, generally, dimensionless functions of the angle of shearing resistance ω.

In the case of foundations in sand c = 0 and

$$p_o = q\, N_q\, \zeta_q + \tfrac{1}{2}\, \gamma\, B\, N_\gamma\, \zeta_\gamma \qquad (3)$$

Using the same general approach but different shear patterns with rupture lines reverting to the shaft (Fig. 3) De Beer (7, 8) and Jaky (9) have obtained another solution of the same problem with considerably higher bearing capacity factors. Their work has been further extended by Meyerhof (10, 11), and others.

All of the previously mentioned solutions were obtained by considering a plane problem (long rectangular foundation). Some work in developing solutions for an axially symmetrical problem (circular foundation) has also been done, primarily in the USSR (12). However, there is still a general tendency to determine the shape factors empirically.

Another possible approach to the problem of base bearing capacity originated in the work by Bishop, Hill and Mott (13), and Skempton, Yassin and Gibson (14), who have considered the problem of expansion of a spherical or cylindrical cavity inside an infinite mass of an ideal solid. In such a case there exists around the cavity a highly stressed zone where the material, by assumption, behaves as a rigid-plastic solid. Outside that zone it behaves as an ideal elastic (or linearly deformable) solid.

The solutions of this kind have been applied to the problem of bearing capacity of deep foundations by Gibson (15), Skempton, Yassin and Gibson (14) and Ladanyi (16). According to these solutions the bearing capacity p_o can be computed by an expression analogous to Eq. 2 without the third term, however. In conditions of infinite mass or of very great depth this third term becomes negligible compared with other two terms. Consequently, both theoretical approaches indicate that at greater depths the bearing capacity of the base should be practically independent of its size and proportional to the overburden pressure q. Based on this conclusion and some limited experimental evidence, it has been generally admitted that the point bearing capacity of pile foundations in sand should be equal to the point resistance of a deep cone penetrometer.

Values of bearing capacity factors N_q found by different theoretical solutions mentioned are shown in Figure 4 left. The diagram on the right shows the corresponding factors $\zeta_q N_q = N_q'$ for circular foundations, as proposed by different investigators. This diagram contains also the empirical curves for N_q recommended by Brinch Hansen (17, 19) and Caquot and Kerisel (18). There is an appreciable difference in proposed numerical values.

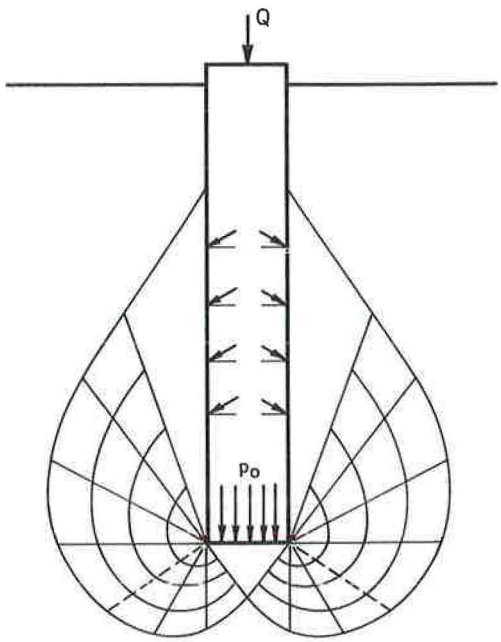

$$p_o = c\, N_c\, \zeta_c + q\, N_q\, \zeta_q + 1/2\, \gamma\, B N_\gamma \zeta_\gamma$$

$$s_o = c_a + K_s \tan \delta\, q_s$$

Figure 3. Shear pattern with rupture lines reverting to the shaft.

The unit skin resistance s_o consists of two terms: one representing adhesion c_a; the other, friction along the skin:

$$s_o = c_a + p_s \tan \delta \tag{4}$$

The term δ denotes the angle of skin friction and p_s average normal pressure on the skin. This pressure is generally assumed to be proportional to the corresponding average overburden pressure along the skin q_s. In sand $c_a = 0$ and

$$p_s = K_s \, q_s \tag{5}$$

K_s is a dimensionless number, which can be called coefficient of skin pressure. With this, the following expression for skin resistance in sand is obtained:

$$s_o = K_s \tan \delta \, q_s \tag{6}$$

Eq. 6 suggests that, in homogeneous soil conditions, unit skin resistance s_o should be proportional to the average overburden pressure q_s.

Previous Experiments

Among numerous experimental studies related to the problem, comparatively few have been of sufficiently general nature to permit drawing definite conclusions concerning the influence of the different parameters involved.

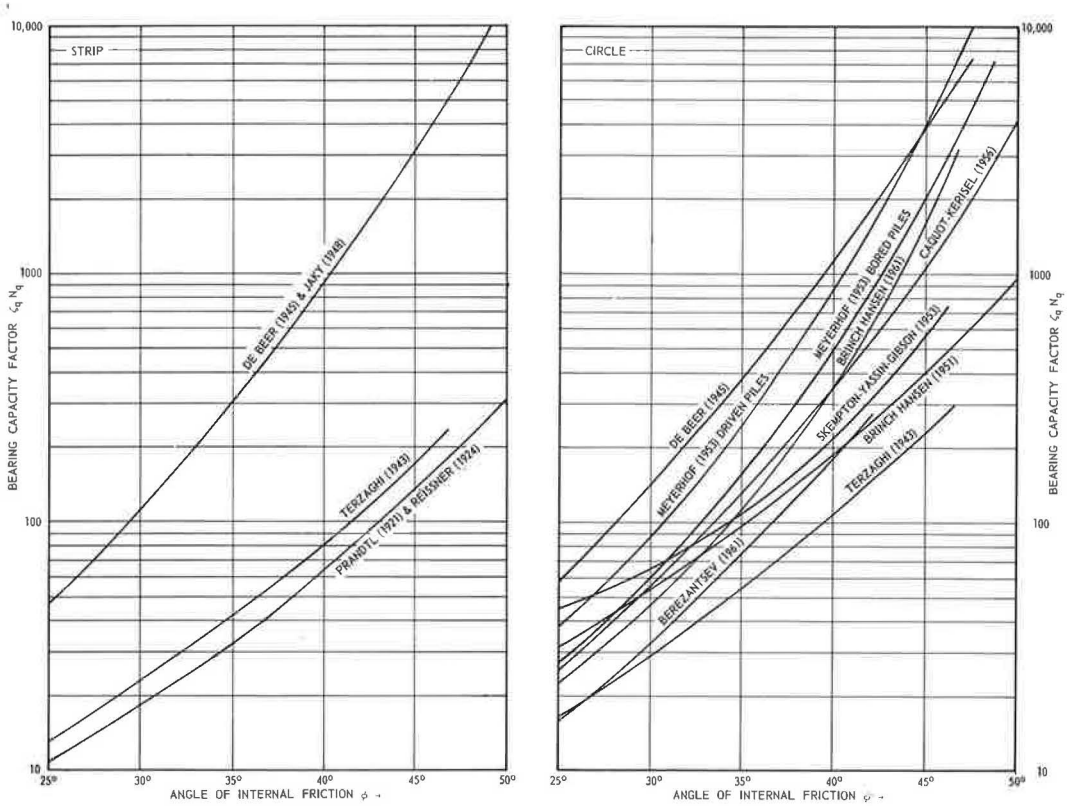

Figure 4. Theoretical bearing capacity factors.

Successful field experiences with predetermination of ultimate bearing capacity of piles by means of deep cone penetration tests (5, 7, 20, 21, 22, 23, 24, 25) have built a certain confidence in the general validity of the theoretical approaches described. It has been found in very many instances that the point bearing capacity of driven piles was indeed comparable to that of a deep cone penetrometer. One of the solutions proposed was being used with apparent success for evaluation of shear strength of sand in situ (8). Also, small-scale model tests (10, 15) as well as several well-documented full-scale tests on piles and piers (32) indicated N_q values in the wide general range predicted by the theories.

Some experiences, however, were not that encouraging. For instance, scale effects of a nature opposite to those predicted by the theories have been reported (26, 27). Observations of shear patterns in sand around deep foundations (28, 29, 30, 31) showed failure surfaces to be localized to the immediate vicinity of the foundation base. To the author's knowledge, not a single test ever indicated failure surfaces reverting to the shaft. The latest large-scale experiments, undertaken by the Institut de Recherches Appliquees du Beton Arme (IRABA) near Paris, led Kerisel (32) to conclude, without a rational explanation, that both foundation depth and size significantly influence the bearing capacity factor N_q. He suggested that N_q was not a unique function of φ but a complex function of φ, D/B and B. This conclusion will be discussed subsequently.

Investigations of the problem were undertaken several years ago with the general aim to contribute, if possible, to the understanding of phenomena occurring beneath and around deep foundations in sand. Both laboratory and field studies were envisaged in different phases of work. As a pilot study, it was proposed to perform large-scale model tests with foundations buried and driven to various depths in uniform masses of sand of different densities. This paper reports on the first phase of the work: tests with buried foundations.

TEST APPARATUS AND MATERIALS

A pile testing facility was constructed adjacent to the Soil Mechanics Laboratory. Figure 5 shows characteristic sections of this facility in different phases of operation. Figure 6 shows a general view.

Test Pit and Loading Equipment

The main feature is a large cylindrical test pit 8 ft 4 in. in diameter and 22 ft deep (Fig. 5), in which models of deep foundations can be placed in any kind of soil under controlled conditions. The pit is connected to a 12-in. sump that allows regulation and control of water level in the models. A 200-ton capacity reaction frame permits vertical or horizontal loading of models by means of corresponding hydraulic jacks. An adjustable A-frame at the upper level serves as support for pile-driving equipment as well as for miscellaneous equipment used in placing and excavating sand for models. This frame permits driving of piles vertically or at any batter up to 3:1 by means of a drop-hammer sliding along the leads. The entire facility is served by a 1.5-ton service crane.

For small-scale tests a steel box 50 by 50 in. square 70 in. deep with a 5-ton loading frame was constructed.

Loading of models was performed generally by means of hydraulic jacks of appropriate capacity (up to 200 tons). The load measurements were made by a corresponding set of proving rings and electronic load cells with a precision of less than 1 percent. Displacement measurements were made by ordinary micrometer dial gages (0.0001-in. precision).

Model Foundations

Two types of foundations were generally built: cylindrical, with circular bases 2.13-, 4- and 6.75-in. diameter, and prismatical, with 2.44- by 12.44-in. rectangular bases. The lengths varied according to the foundation depths (Table 1) between 10 and 113 in.

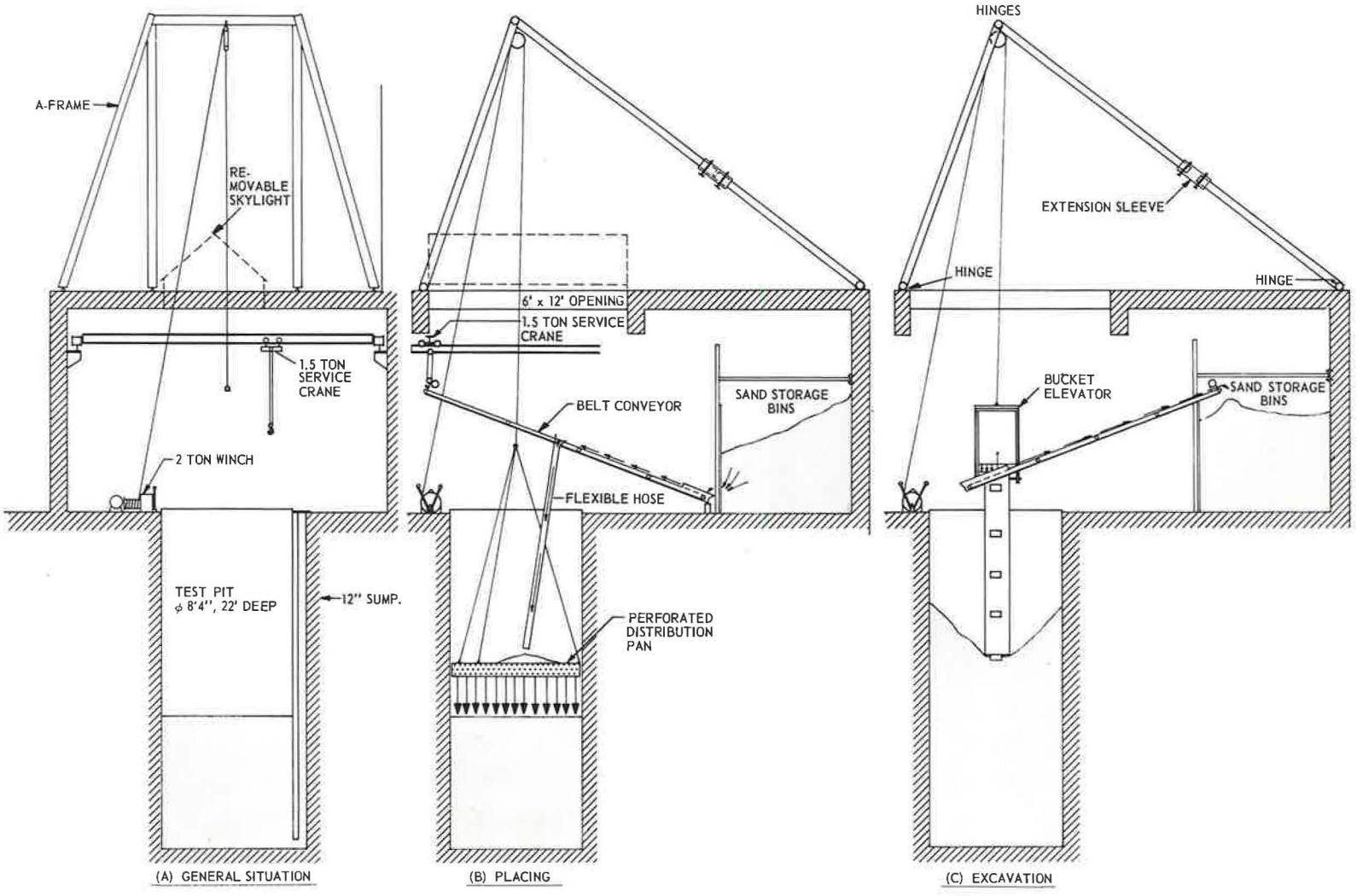

Figure 5. Testing area in different phases of operation.

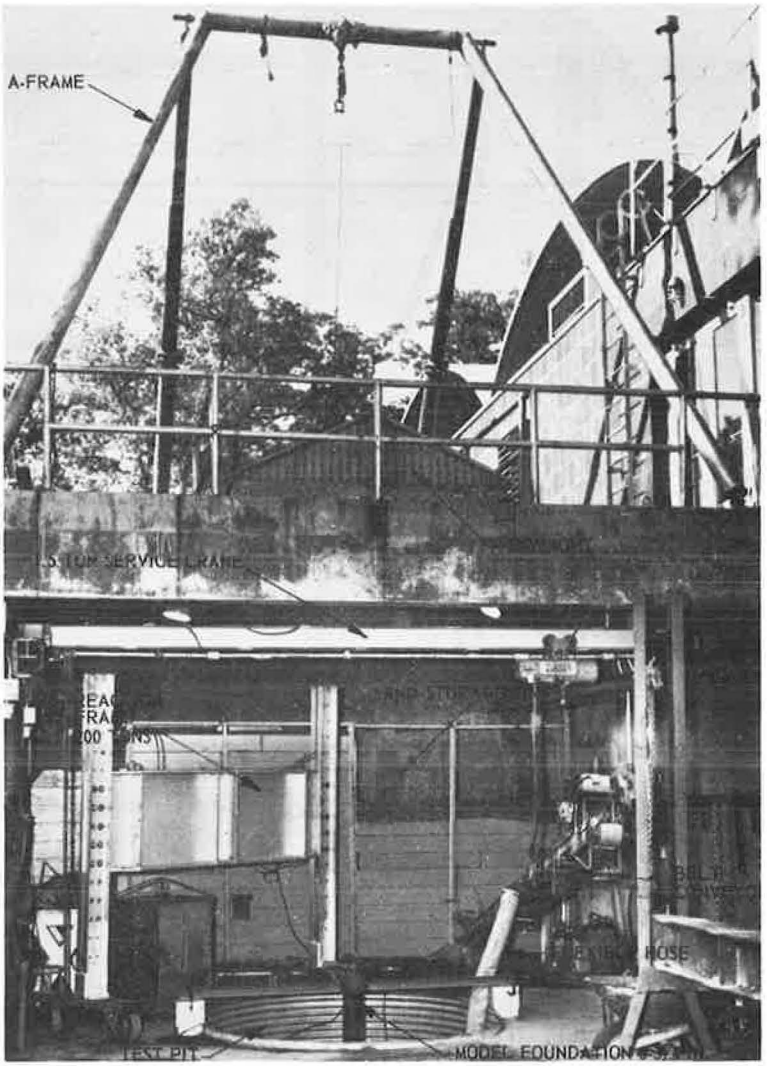

Figure 6. Testing area.

TABLE 1

SUMMARY OF LOADING TESTS

Series	Test Numbers	Foundation			Different Sand Densities	Container Size (in.)
		Shape	Size (in.)	Depth (in.)		
A[a]	21 - 40	Circular	2.13	0, 10, 20 30, 40	4	50 × 50 × 70
B[b]	1 - 20	Rectangular	2 × 12	0	4	50 × 50 × 70
			2.44 × 12.44	10, 20 30, 40		
C	41 - 52	Circular	3.94	0	4	50 × 50 × 70
			4	40		
				80	3	100ϕ, 264
D	61 - 70	Circular	6	0	4	100ϕ, 264
			6.75	60, 100	3	
E	81 - 84	Circular	8	0	4	100ϕ, 264

[a] Skin diameter, 2 in.
[b] Skin dimensions, 2.25 × 12.25 in.

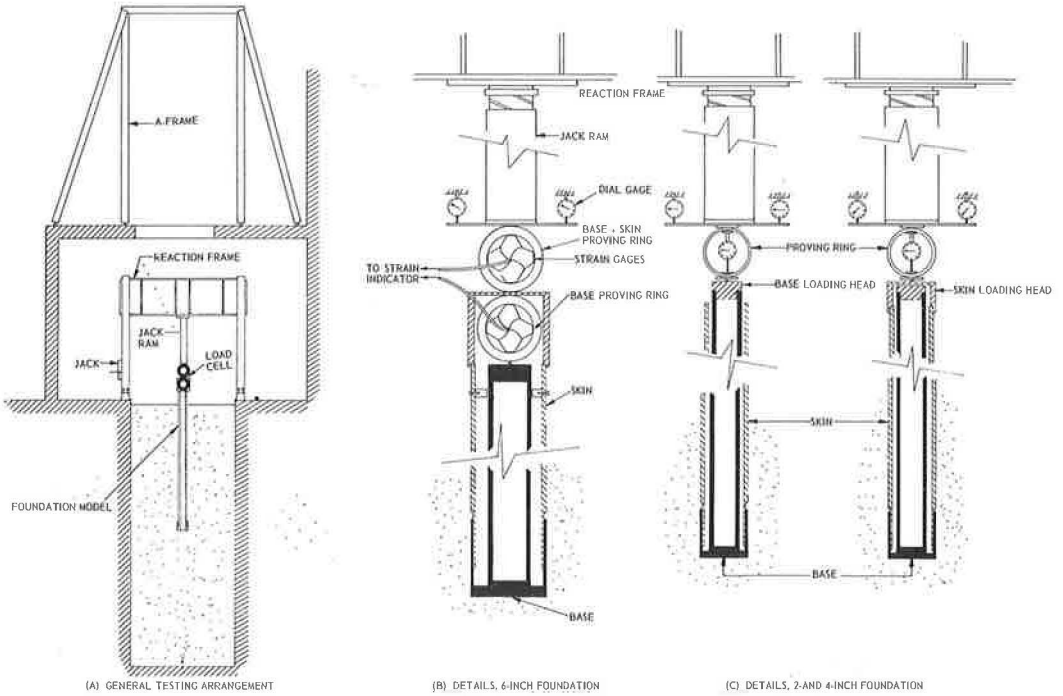

Figure 7. Model foundations.

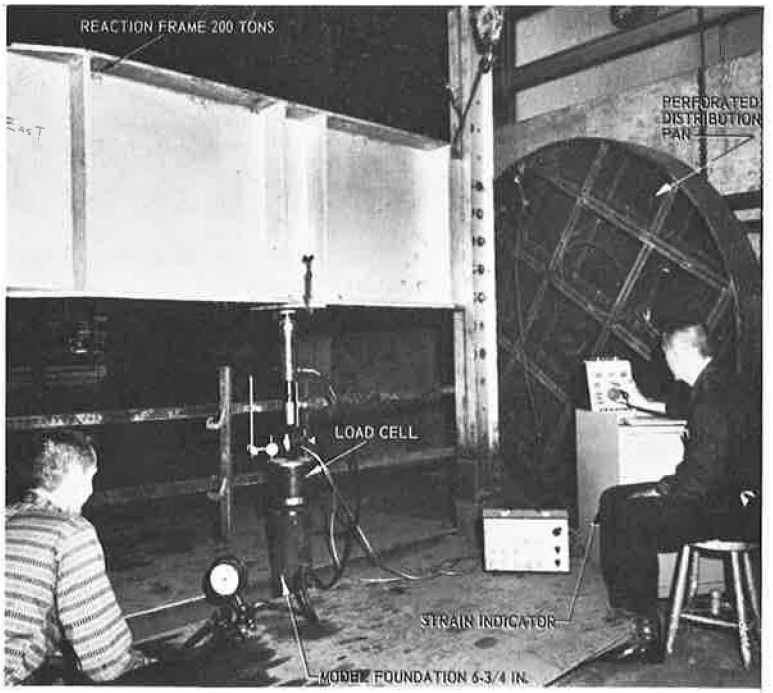

Figure 8. Test in progress.

The foundations were constructed on a principle similar to that of a deep cone penetrometer. They consist of a steel casing inside which a steel shaft independently connects the loading head with the base. In the case of 2- and 4-in. diameter foundations (Fig. 7) separate loading of base and skin of the foundation is possible through exchange of the loading head. In the case of 6-in. diameter foundations (Fig. 7b) the loading head is constructed so as to allow separate registration on the strain-indicator of base and total (base + skin) load. Figure 8 shows an outside view of this special head.

The flat bearing surfaces of the bases are covered by sandpaper to assure perfect roughness. To prevent caving-in of sand while the base only is pushed, the latter is protected by a cap tightly fitted with the bottom of the casing. To minimize friction between the cap and casing, the contact surface is kept clean and perfectly lubricated.

Properties of Sand

All the tests in this investigation were performed with a medium sand originating from the Chattahoochee River, near Atlanta. The sand was sieved through a window screen (equivalent to 1.44-mm sieve opening). The grain size distribution curve (Fig. 9) and microscopic examinations indicate a medium, uniform sand composed mostly of subangular quartz particles, but rich in mica. The material has been air-dried prior to use in tests. The water content, controlled throughout the investigation, varied between 0.2 and 0.3 percent.

Maximum and minimum densities of this sand, as determined by standard procedures are given in Table 2, which also contains corresponding minimum and maximum porosities n and void ratios e.

Shear strength characteristics of the sand were determined by standard triaxial tests (constant cell pressure and positive deviator stress). A total of 54 air-dry samples 2.8 in. in diameter and approximately 6 in. high were prepared at four different densities, and tested using cell pressures varying from 5 to 80 psi. A strain-controlled loading machine was used for all the tests with the axial strain rate 0.02 in. per min (Table 3).

Assuming the Coulomb-Mohr criterion of failure to be valid, an ordinary plot of these results in τ vs σ or $\sigma_1 - \sigma_3$ vs $\sigma_1 + \sigma_3$ presentation can be made. Such a plot indicated that the strength envelopes of the sand in question are slightly curved. For better insight into the nature of this curvature the results are also plotted as $\sigma_1 - \sigma_3$ vs $1/\sigma_3$, a plot proposed by Hansen and Odgaard (33). In such a presentation a straight-line strength envelope appears as a straight line having the equation

$$\frac{\sigma_1 - \sigma_3}{\sigma_3} = \frac{2 \sin \varphi}{1 - \sin \varphi} + \frac{2 \cos \varphi}{1 - \sin \varphi} \frac{c}{\sigma_3} \qquad (7)$$

Figure 10 shows that a reasonably good straight-line approximation of the actually curved envelopes can be obtained by separately considering tow ranges of confining pressures σ_3, namely, $\sigma_3 < 10$ psi and $\sigma_3 > 10$ psi.

For $\sigma_3 < 10$ psi ($1/\sigma_3 > 0.10$ psi) the $\sigma_1 - \sigma_3/\sigma_3$ values are practically independent of $1/\sigma_3$, which means that the shear strength intercept c_0 is zero. The angles of internal friction φ_0 corresponding to observed shear strengths are given in Table 2 (Col. 9) and plotted in Figure 11, which shows that φ_0 can be expressed as a function of e approximately by

$$\tan \varphi_0 = \frac{0.68}{e} \qquad (8)$$

For 80 psi $> \sigma_3 >$ 10 psi the $\sigma_1 - \sigma_3/\sigma_3$ values can be approximated by linear functions of $1/\sigma_3$; which indicates that the shear strength intercept c_1 is different from zero. Table 2 (Cols. 10 and 11) gives values in-

TABLE 2

MINIMUM AND MAXIMUM DENSITIES OF CHATTAHOOCHEE RIVER SAND

Density	Dry Unit Weight (pcf)	Void Ratio, e	Porosity n (%)
Minimum	79.0	1.10	52.4
Maximum	102.5	0.615	38.1

TABLE 3

TRIAXIAL TEST RESULTS

Test No.	γ_d (pcf)	Void Ratio, e	Mean Void Ratio	Cell Pressure, σ_3 (psi)	Stress Difference at Failure, $\sigma_1 - \sigma_3$ (psi)	Axial Strain at Failure (%)	$\frac{\sigma_1 - \sigma_3}{\sigma_3}$	Angle of Internal Friction, φ_0	Strength Intercept, c_0 (psi)	Angle of Internal Friction, φ_0	Strength Intercept, c_1 (psi)
(1)	(2)	(3)	(4)	(5)	(6)	(7)	(8)	(9)	(10)	(11)	(12)
1	84.6	0.957		5	13.3	2.7	2.65				
2	84.6	0.952		10	27.4	7.6	2.74				
3	84.6	0.957		10	31.0	4.6	4.10				
4	84.4	0.961		20	49.1	6.6	2.46				
6	84.0	0.970	0.957	40	90.4	11.9	2.26	35° 20'	0	32°	1.08
8	84.6	0.957		80	182.0	8.1	2.28				
34	85.1	0.945		10	24.5	13.2	2.45				
40	84.6	0.957		40	96.0	7.4	2.40				
46	84.4	0.96		7	18.3	3.8	2.62				
47	84.6	0.956		7	20.6	2.8	2.94				
48	84.7	0.955		5	14.5	2.4	2.90				
5	90.5	0.830		20	62.2	4.6	3.11				
7	90.1	0.838		40	117.3	9.3	2.93				
11	89.6	0.847		5	16.9	2.9	3.39				
12	90.1	0.838		10	32.6	4.5	3.26				
13	90.1	0.838	0.836	20	62.4	8.2	3.12	38° 40'	0	35° 10'	1.55
14	90.1	0.838		40	108.6	10.7	2.72				
15	90.5	0.830		10	40.5	4.4	4.05				
31	91.3	0.813		20	60.1	6.4	3.00				
32	90.3	0.833		40	118.3	9.6	2.96				
33	90.5	0.830		55	156.2	9.4	2.84				
35	90.7	0.827		10	34.0	7.0	3.40				
38	89.0	0.859		40	115.7	6.4	2.89				
49	90.1	0.838		7	22.8	4.0	3.26				
50	90.2	0.836		7	25.0	3.4	3.57				
51	90.1	0.838		5	15.9	3.0	3.18				
16	94.8	0.747		5	22.5	3.0	4.51				
17	94.5	0.751		10	43.1	4.5	4.31				
18	95.0	0.742		20	78.3	6.7	3.92				
19	95.4	0.737		40	142.0	7.1	3.55				
20	95.4	0.737	0.745	75	247.9	9.2	3.30	42° 50'	0	38° 20'	2.42
39	94.3	0.755		35	125.7	4.6	3.60				
52	94.8	0.747		7	28.3	3.8	4.04				
53	94.9	0.745		7	31.0	3.0	4.44				
54	95.0	0.742		5	20.5	3.1	4.10				
21	97.9	0.691		5	24.3	5.0	4.87				
22	98.8	0.676		10	48.2	4.3	4.82				
23	98.7	0.678		20	79.4	5.4	3.97				
24	98.5	0.681		35	140.9	7.9	4.02				
25	98.7	0.678	0.681	70	250.7	9.8	3.58	45°	0	40°	2.85
26	98.6	0.680		40	146.1	8.9	3.65				
36	98.2	0.685		10	48.7	4.8	4.87				
41	98.5	0.681		5	23.5	3.0	4.87				
42	98.7	0.678		10	47.0	3.2	4.70				
43	98.5	0.681		20	83.2	6.7	4.16				
44	98.6	0.680		7	32.6	3.6	4.66				
45	98.4	0.682		7	34.1	3.9	4.87				

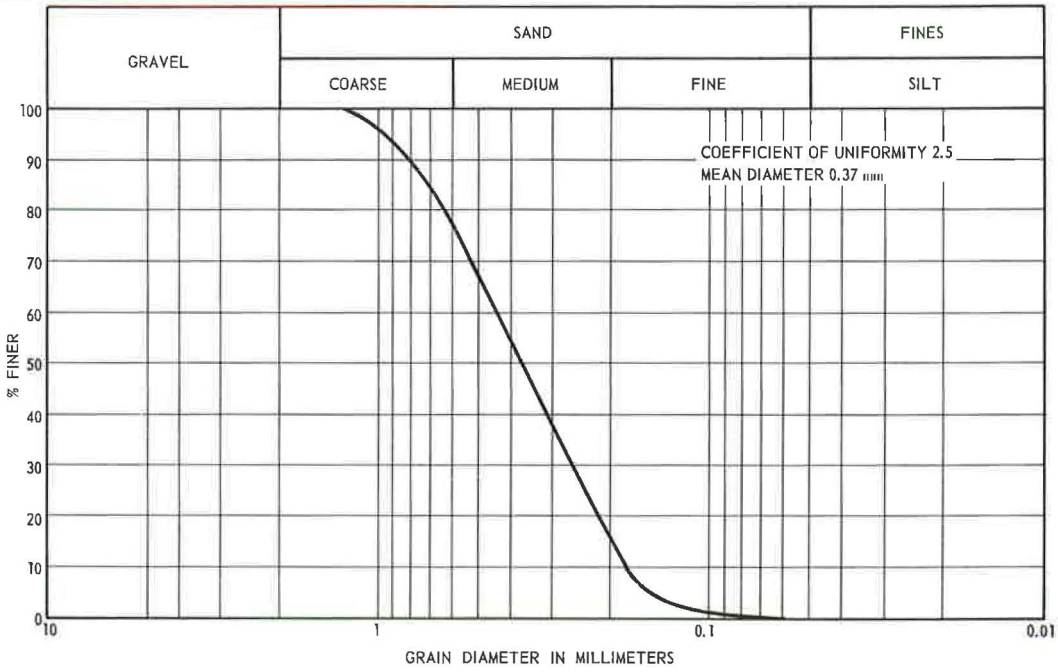

Figure 9. Grain-size distribution curve.

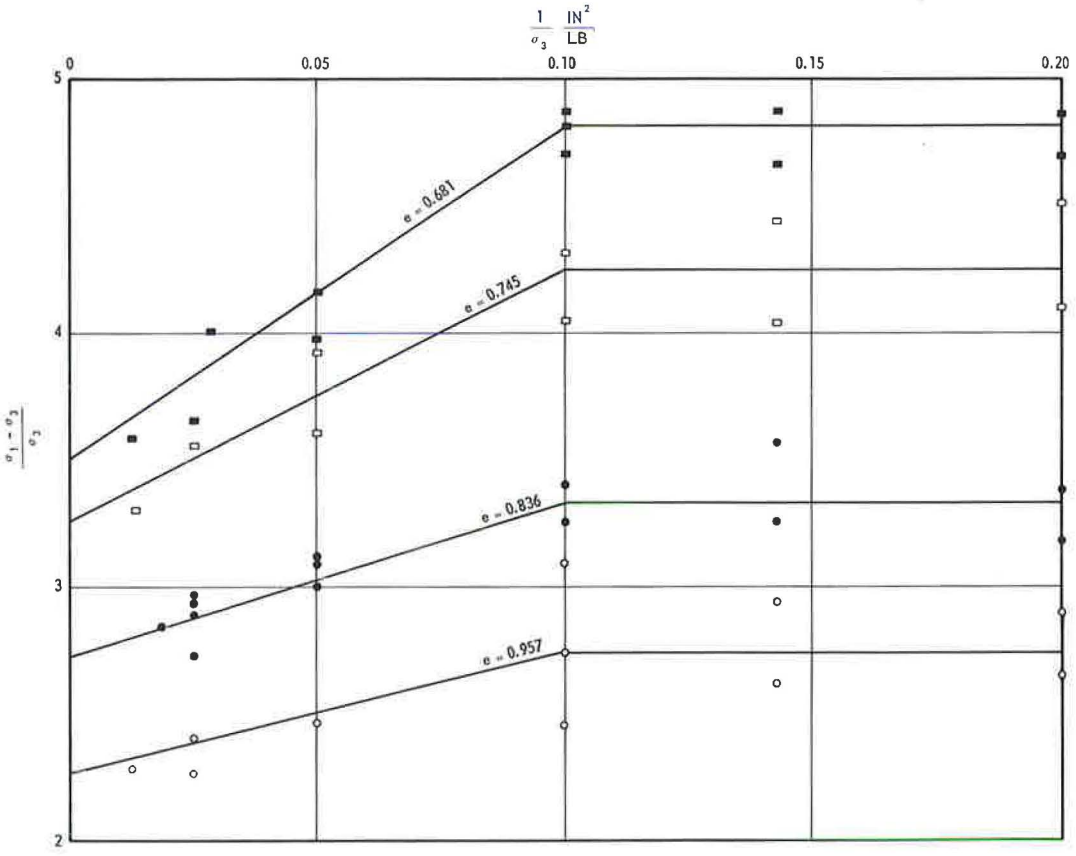

Figure 10. Triaxial test results.

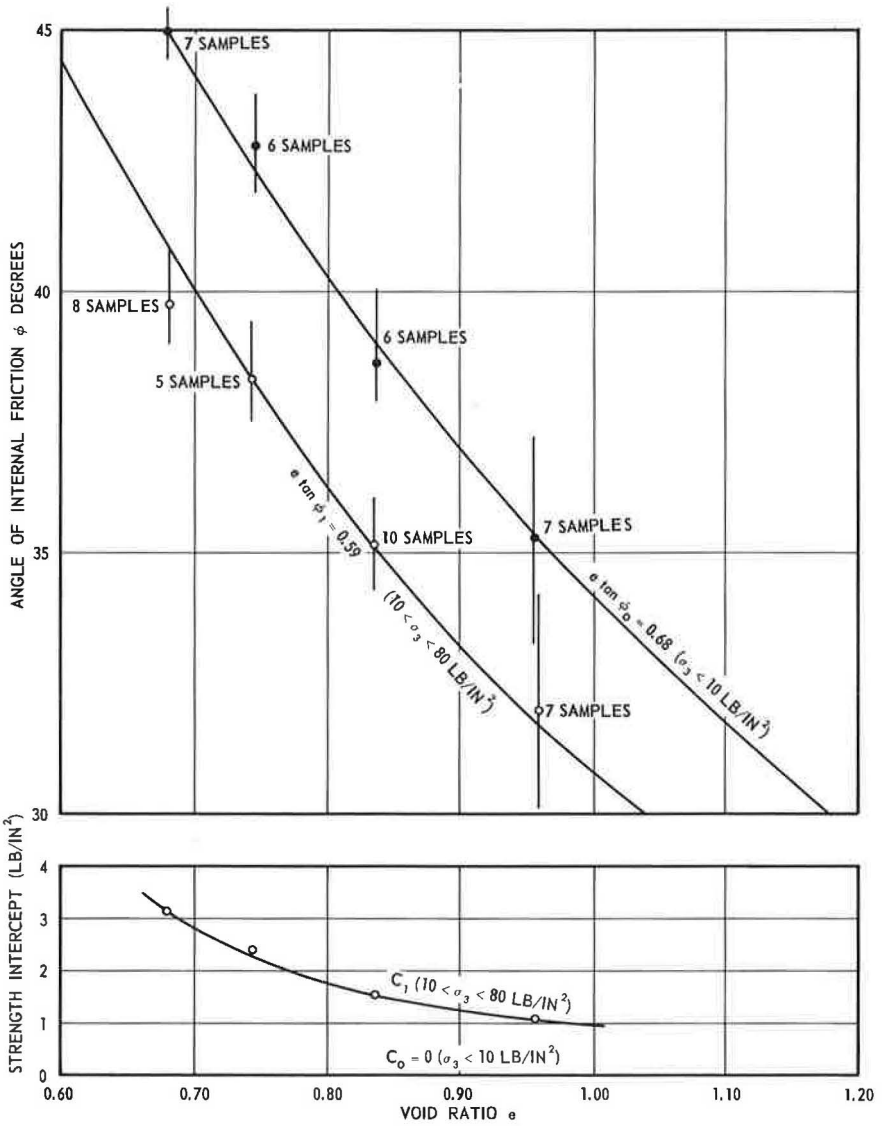

Figure 11. Shear strength parameters as a function of initial void ratio.

dicated by Figure 10 (left). The same c_1 and φ_1 values as functions of initial void ratio e are shown in Figure 11. The following analytical expression gives a good approximation of φ_1 as a function of e:

$$\tan \varphi_1 = \frac{0.59}{e} \tag{9}$$

DESCRIPTION OF TESTS

Placing of Sand and Control of Density

All the models for this investigation have been constructed in the following way. First, sand of desired uniform density was placed up to the planned elevation of the foundation base. The model foundation was then brought to full contact with the care-

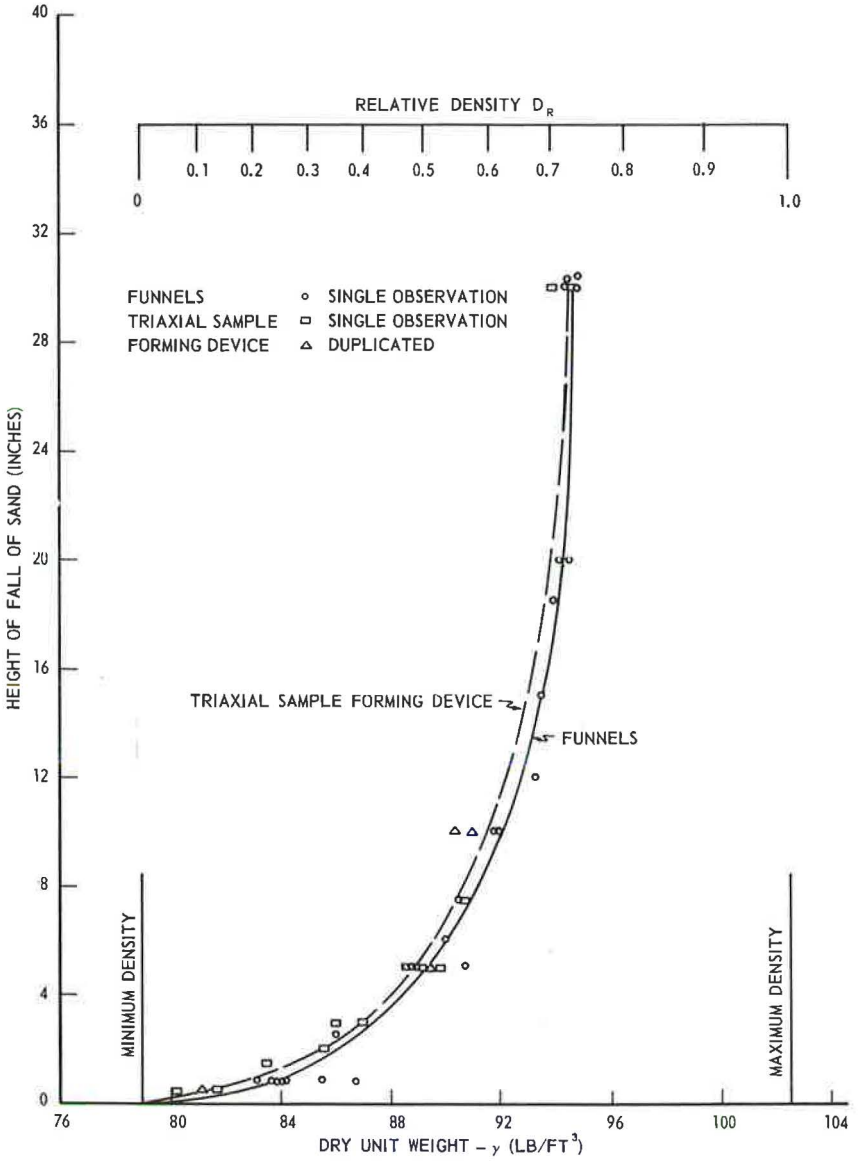

Figure 12. Relative density of sand as function of height of fall.

fully prepared horizontal sand surface and fixed in place so that it could not move during the subsequent operation of filling the sand above the base of the footing. Following former experience (34), exceptionally uniform loose- and medium-dense sand models (D_R < 0.70) were built by pouring sand from containers with perforated bottoms (Fig. 5b). It was confirmed again that the density of sand models so built is a unique function of the height of free fall of sand as long as other variables (rate of flow) remain the same (Fig. 12).

Denser sand models (D_R > 0.70) were built by surface vibration of 4-in. thick sand layers obtained by pouring sand 30 in. from the perforated container. Electric vibrators with a frequency of 3,600 cpm, attached to steel plates of appropriate shape, were used for surface vibration. Lead surcharge was added as necessary to achieve maxi-

mum compaction. All possible care was exercised to obtain uniform density throughout a model.

The homogeneity of sand in models was checked by penetrometer soundings. A simple static-cone micropenetrometer was constructed. This device has a $\frac{1}{2}$-in. point diameter and a $\frac{3}{8}$-in. shaft diameter of the casing. The assembly can be pushed into the sand by means of a screw jack at about 4 in. per min. Total resistance (point + skin) was recorded in several positions across the model and plotted against depth for each test. To convert the measurements of this kind into density, an empirical relationship was established between total resistance reduced to unit area of the point end dry unit weight of the material (Fig. 13). This was achieved by sounding sand models in a 24- by 16- by 60-in. box placed on a scale and filled by the same methods as used for building larger models.

Review of Tests Performed

Following the previously outlined program, six series of tests were performed. The main characteristics of five series of regular loading tests are given in Table 1.

The sixth series of tests, Series M, numbered 101 to 105, was devoted to the study of failure phenomena under foundations. Models of soil were built of distinct layers of sand to which cements of two different colors were added (10% by weight). After performing the loading test in the usual way, water was added to the models to cause setting of the layered mass. A few days later, the hardened block was cut through characteristic sections where shear patterns at failure were visible for observation and analysis.

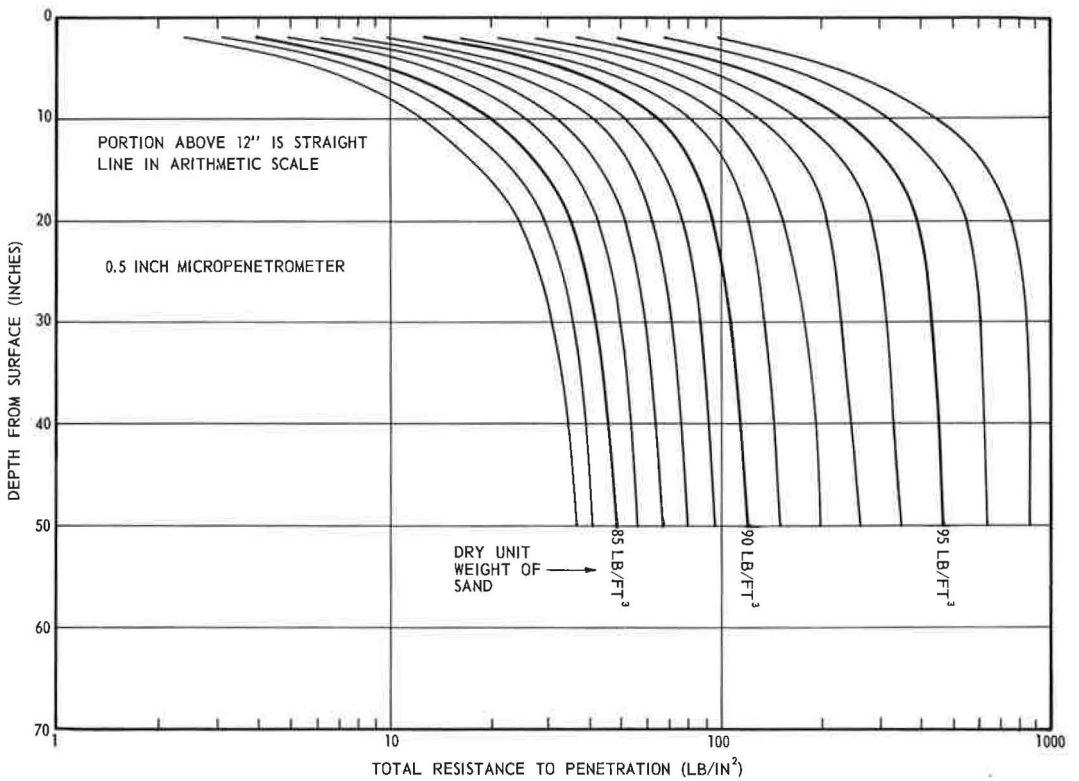

Figure 13. Relationship between depth and total penetration resistance for different sand densities.

Loading Procedure

The loading procedure for tests at the surface was similar to that followed in ordinary plate load tests. The load was applied in increments of about $1/20$ of the estimated failure load at 1-min intervals.

The loading procedure for tests beneath the surface was, in principle, the same. However, three separate loading stages existed in each test of series A, B and C. First, the foundation base was pushed until failure was reached; second, the same procedure was repeated with the foundation shaft; and third, after the shaft reached the base, both were pushed together and the total resistance was recorded.

Inasmuch as the loading head of the 6.75-in. foundations was of different construction (Fig. 7), the loading stages in D-tests differed somewhat from those just described. By pushing the foundation base to failure, the loading head was brought to contact with the skin and the entire foundation was forced into the soil. Special proving rings (Fig. 7) registered base and skin loads separately during this second stage.

Displacements of foundation base and skin were recorded at 1-min intervals by two micrometer dial gages placed near the loading head (Fig. 7). Also, in tests of series D, displacements of the sand surface were measured at different locations around the foundation.

TEST RESULTS

Significant results of the loading tests performed are given in Tables 4 through 9. Characteristic load-settlement diagrams of surface tests are shown in Figures 14 through 16. The black points indicate ultimate and first failure loads. The criterion by which these loads were established will be discussed subsequently.

Characteristic load-settlement diagrams of base and skin loading tests at greater depth are shown in Figures 17 through 19 and 20 through 22. Black points indicate ultimate loads.

Characteristic failure patterns at greater depth obtained in tests with colored sand are shown in Figures 23 through 25. Figure 23 shows what happens when a circular shaft penetrates through dense sand ($D_R \sim 0.9$) from a relative depth of $D/B = 10$ to a relative depth of $D/B = 19$. Figure 24 shows the analogous phenomenon for a rectangular foundation penetrating from $D/B = 10$ to $D/B = 11$, and Figure 25 for a rectangular foundation penetrating from $D/B = 5$ to $D/B = 6$.

Types of Failure

Three characteristic types of failure were observed in surface tests. Foundations on relatively dense sand ($D_R > 0.70$) fail suddenly with very pronounced peaks of base resistance (Fig. 26a) when the settlement reaches about 7 percent of the foundation width. The failure is accompanied by the appearance of failure surfaces at the sand surface and by considerable bulging of sheared mass of sand. The phenomenon corresponds exactly to that described earlier by Terzaghi (6) as "general shear failure."

Foundations on sand of medium density ($0.35 < D_R < 0.70$) do not show a sudden failure. As the settlements exceed about 8 percent of the foundation width small sudden shears within the sand mass are apparent from observations of load and settlement gages. Simultaneously, bulging of the sand surface starts. At settlements of about 15 percent of foundation width, a visible boundary of sheared zone at the sand surface appears. However, the peak of base resistance may never be reached.

The phenomenon is of the same nature as that described by Terzaghi (6) and by De Beer and Vesić (34) as "local shear failure" (rupture par refoulement incomplet). In the latter investigation, however, the tests were stress-controlled, so that the beginning of large shears in the soil mass was much more pronounced and was always recorded as the first failure of the foundation.

Finally, foundations on relatively loose sand ($D_R < 0.35$) penetrate into the soil without any bulging of the sand surface (Fig. 26c). The base resistance steadily increases as the settlement progresses. The rate of settlement, however, increases and reaches a maximum at a settlement of about 15 to 20 percent of foundation width.

TABLE 4

SIGNIFICANT RESULTS OF LOADING TESTS WITH CIRCULAR PLATES AT THE SURFACE

Test No.	Plate Diameter, B (in.)	Dry Unit Weight of Sand, γ_d (pcf)	Ultimate Pressure, p_o (psi)	$\frac{p_o}{\frac{1}{2}\gamma B}$	Ultimate Settlement, w (psi)	$\frac{w}{B}$ (%)	Type of Failure[a]
(1)	(2)	(3)	(4)	(5)	(6)	(7)	(8)
34	2.13	96.0	33.8	572	0.126	5.9	G
21	2.13	93.0	10.2 (7.6)[b]	173 (129)	0.272	12.8	L
22	2.13	89.8	7.4 (3.9)	134 (70.6)	0.414	19.5	L
23	2.13	82.6	2.4 (0.8)	48.2 (15.0)	0.463	21.8	P
44	3.94	96.7	53.8	432	0.227	5.8	G
41	3.94	93.8	19.8 (13.4)	186 (126)	0.446	11.3	L
42	3.94	91.0	13.0 (6.7)	126 (64.7)	0.621	19.2	L
43	3.94	83.3	3.1 (1.6)	32.5 (16.3)	0.582	14.8	P
61	6.00	96.2	73.4	432	0.425	7.1	G
62	6.00	93.0	31.0 (23.0)	193 (143)	0.869	14.5	L
63	6.00	91.7	19.3 (13.6)	121 (85.5)	0.875	14.6	L
64	6.00	95.0	5.3 (3.3)	35.9 (22.1)	0.852	14.2	P
84	8.00	96.2	79.2	432	0.667	8.3	G
81	8.00	95.2	55.9	262	0.737	9.2	G
82	8.00	95.2	42.1	193	0.695	8.7	G
83	8.00	88.0	9.0 (7.0)	44.2 (34.4)	1.08	13.5	L

TABLE 5

SIGNIFICANT RESULTS OF LOADING TESTS WITH RECTANGULAR PLATES AT THE SURFACE

Test No.	Plate Size (in.)	Dry Unit Weight of Sand, γ_d (pcf)	Ultimate Pressure, p_o (psi)	$\frac{p_o}{\frac{1}{2}\gamma B}$	Ultimate Settlement, w (in.)	$\frac{w}{B}$	Type of Failure[a]
(1)	(2)	(3)	(4)	(5)	(6)	(7)	(8)
16	2 × 12	96.4	47.0	842	0.212	10.6	G
1	2 × 12	93.6	22.1 (14.8)[b]	268	0.397	19.9	L
2	2 × 12	91.9	11.6 (8.3)	147	0.403	20.1	L
3	2 × 12	84.0	2.1 (1.4)	28.8	0.429	21.4	P

[a] G = general shear; L = local shear; P = punching shear.
[b] Numbers in parentheses refer to first failure.

TABLE 6

SIGNIFICANT TEST RESULTS – CIRCULAR DEEP FOUNDATIONS[a]

Test No.	Depth, D (in.)	Dry Unit Weight of Sand, γ_d (pcf)	Ultimate Base Resistance, p_o (psi)	Ultimate Settlement, w (in.)	$\frac{w}{B}$ (%)	Ultimate Skin Resistance, s_o (psi)	Ultimate Skin Displacement (in.)	Total Ult. Load (lb)	Ult. Displacement for Total Load (in.)
(1)	(2)	(3)	(4)	(5)	(6)	(7)	(8)	(9)	(10)
37	10	96.5	238.0	0.315	14.8	0.582	0.352	850	0.22
24		92.0	62.5	0.560	26.3	—	—	—	—
25		90.0	41.1	0.574	27.0	0.332	0.115	173	0.13
26		83.5	14.1	0.434	20.4	0.267	0.249	57	0.06
38	20	96.4	298.0	0.447	21.0	1.020	0.420	1,340	0.39
27		93.8	99.2	0.633	29.8	0.342	0.352	477	0.18
28		91.5	54.1	0.625	29.4	0.341	0.385	290	0.28
29		82.8	14.3	0.425	20.0	0.314	0.344	93	0.10
39	30	96.2	329.0	0.429	20.2	1.618	0.704	1,730	0.28
30		94.0	112.5	0.703	33.1	0.412	0.330	540	0.20
31		91.3	61.6	0.616	29.0	0.350	0.294	287	0.17
32		84.2	20.2	0.483	22.7	0.264	0.270	126	0.07
40	40	95.9	302.0	0.459	21.6	1.653	0.757	1,670	0.18
33		93.3	113.8	0.623	29.3	0.366	0.362	572	0.22
34		90.9	73.1	0.561	26.4	0.331	0.335	323	0.21
35		82.4	17.4	0.474	22.3	0.238	0.315	144	0.10

[a]Base diameter, 2.13 in.; skin diameter, 2.00 in.

TABLE 7

SIGNIFICANT TEST RESULTS – CIRCULAR DEEP FOUNDATIONS[a]

Test No.	D (in.)	γ_d (pcf)	p_o (psi)	w (in.)	$\frac{w}{B}$ (%)	Ult. Skin Resistance, s_o (psi)	Ult. Skin Displacement (in.)	Total Ult. Load (lb)	Ult. Displacement for Total Load (in.)
(1)	(2)	(3)	(4)	(5)	(6)	(7)	(8)	(9)	(10)
48	40	95.8	202.0	0.933	23.3	1.002	0.251	3,370	0.30
45		94.6	114.9	0.971	24.3	0.484	0.348	1,990	0.30
46		91.1	62.0	1.126	28.2	0.465	0.362	1,010	0.23
47		83.8	26.3	1.174	29.4	0.400	0.462	515	0.22
51	80	94.8	184.0	0.941	23.5	2.260	0.267	4,260	0.30
49		93.8	130.8	1.417	35.4	0.793	0.300	2,340	0.19
50		82.3	27.8	1.073	26.8	0.454	0.376	800	0.39

[a]Base and skin diameter, 4.00 in.

TABLE 8

SIGNIFICANT TEST RESULTS – CIRCULAR DEEP FOUNDATION[a]

Test No.	D (in.)	γ_d (pcf)	p_o (psi)	w (in.)	w/B (%)	Ult. Skin Resistance, s_o (psi)	Ult. Skin Displacement (in.)	Total Ult. Load (lb)
(1)	(2)	(3)	(4)	(5)	(6)	(7)	(8)	(9)
68	60	96.5	341.6	2.17	32.2	1.700	0.350	14,000
69		94.0	98.8	1.88	27.8	0.491	0.330	3,950
70		84.1	30.6	1.26	18.7	0.430	0.380	1,570
67	110	95.6	271.0	2.20	32.6	1.750	0.421	12,800
65	113	91.8	96.4	2.90	43.0	0.683	0.350	4,700
66	110	85.8	55.8	1.81	26.8	—	—	2,830

[a]Base and skin diameter, 6.75 in.

TABLE 9

SIGNIFICANT TEST RESULTS – RECTANGULAR DEEP FOUNDATIONS[a]

Test No.	Depth, D (in.)	Dry Unit Weight of Sand, γ_d (pcf)	Ult. Pressure, p_o (psi)	Ult. Displacement, w (in.)	$\frac{w}{B}$ (%)	Ult. Skin Resistance, s_o (psi)	Ult. Skin Displacement (in.)	Total Ult. Load (lb)	Ult. Displacement for Total Load (in.)
(1)	(2)	(3)	(4)	(5)	(6)	(7)	(8)	(9)	(10)
17	10	95.0	126.0	0.605	24.4			3,140	0.23
4		94.0	52.8	0.600	24.6			1,550	0.18
5		91.1	32.4	0.712	29.2			1,050	0.10
6		83.8	8.8	0.594	24.3			420	0.10
18	20	95.1	159.8	0.626	25.7	0.299	0.222	4,810	0.41
7		93.8	79.5	0.766	31.4	0.168	0.268	2,610	0.25
8		90.9	39.4	0.689	28.2	0.174	0.165	1,570	0.18
9		82.0	11.1	0.657	26.9	0.124	0.124	560	0.18
19	30	96.4	181.5	0.715	29.3	0.484	0.235	6,190	0.40
10		94.2	84.2	0.740	30.3	0.282	0.197	3,000	0.27
11		91.8	48.4	0.759	31.1	0.208	0.185	2,000	0.29
12		82.0	11.9	0.566	22.8	0.153	0.170	705	0.22
20	40	96.5	188.6	0.600	24.6	0.673	0.152	6,500	0.40
13		94.1	85.2	0.700	28.7	0.270	0.118	3,320	0.40
14		90.7	45.0	0.700	28.7	0.210	0.125	1,980	0.22
15		82.0	11.5	0.373	15.3	0.188	0.162	735	0.08

[a]Base width, 2.44 in.; base length, 12.44 in.; skin width, 2.25 in.; skin length, 12.25 in.

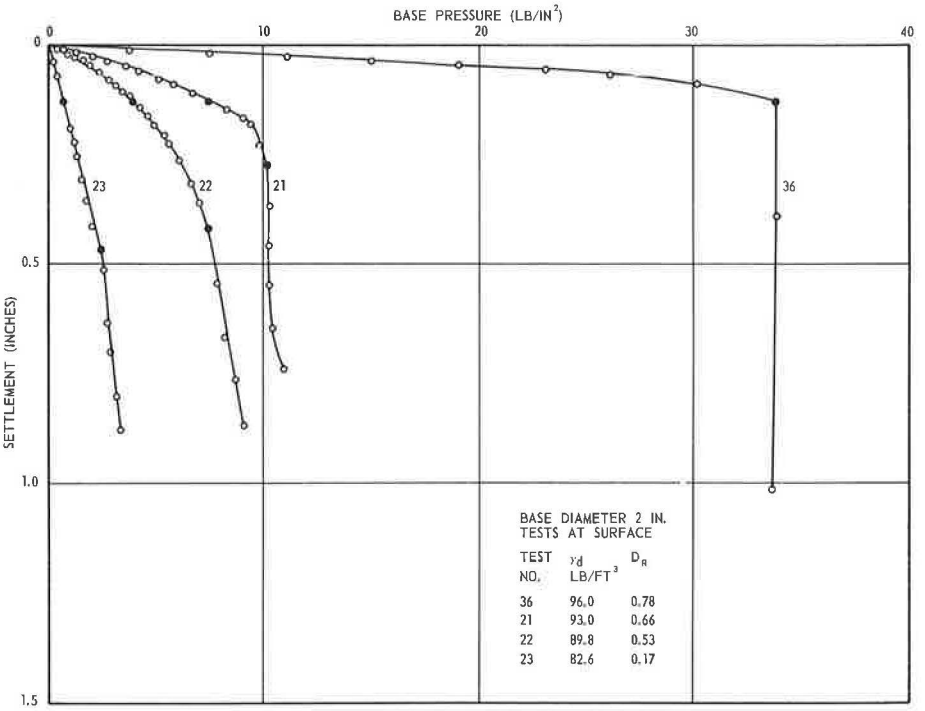

Figure 14. Typical results of surface tests.

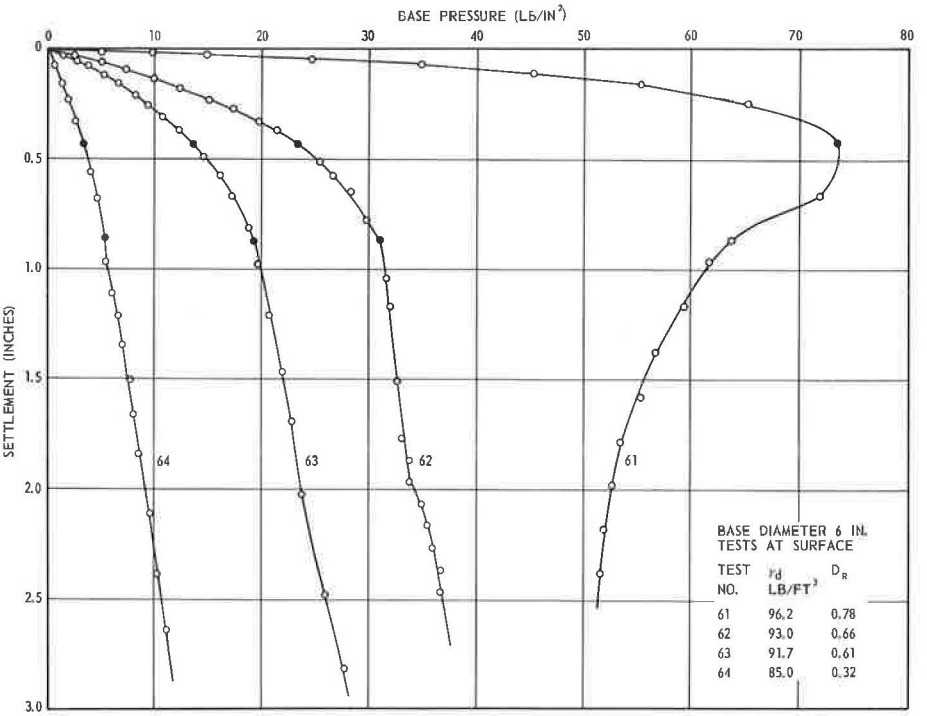

Figure 15. Typical results of surface tests.

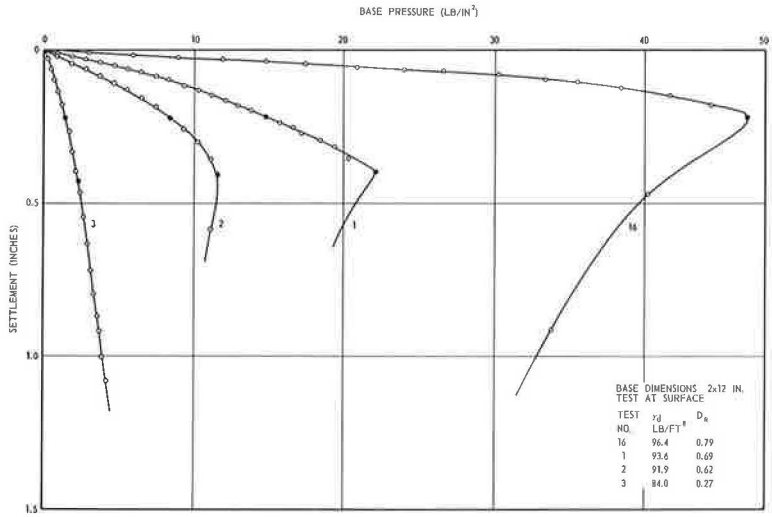

Figure 16. Typical results of surface tests.

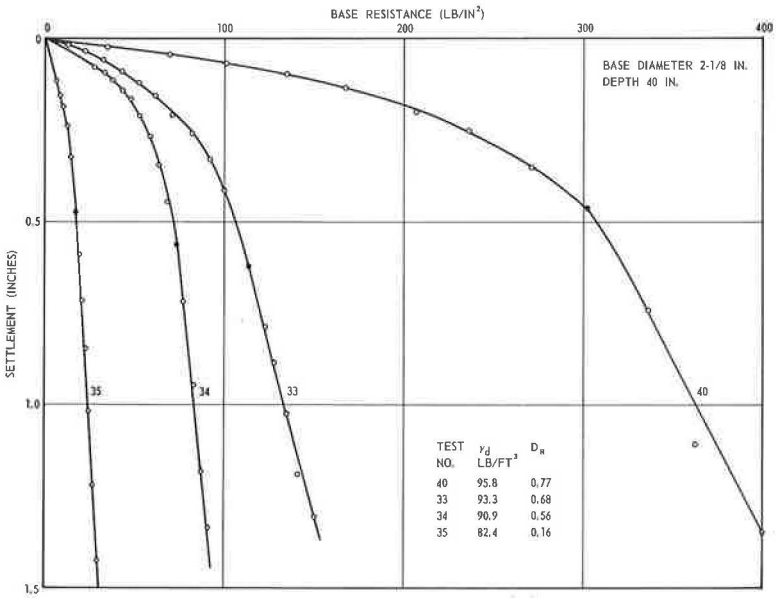

Figure 17. Typical results of base loading tests at greater depth.

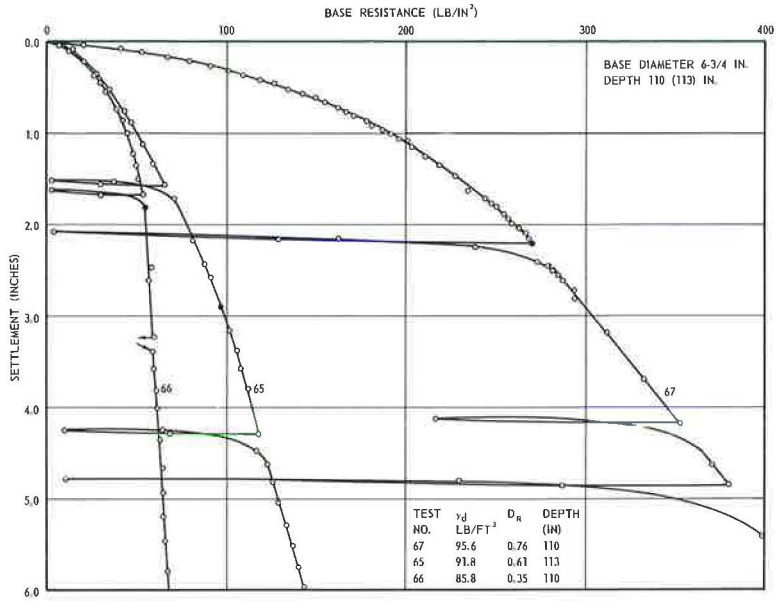

Figure 18. Typical results of base loading tests at greater depth.

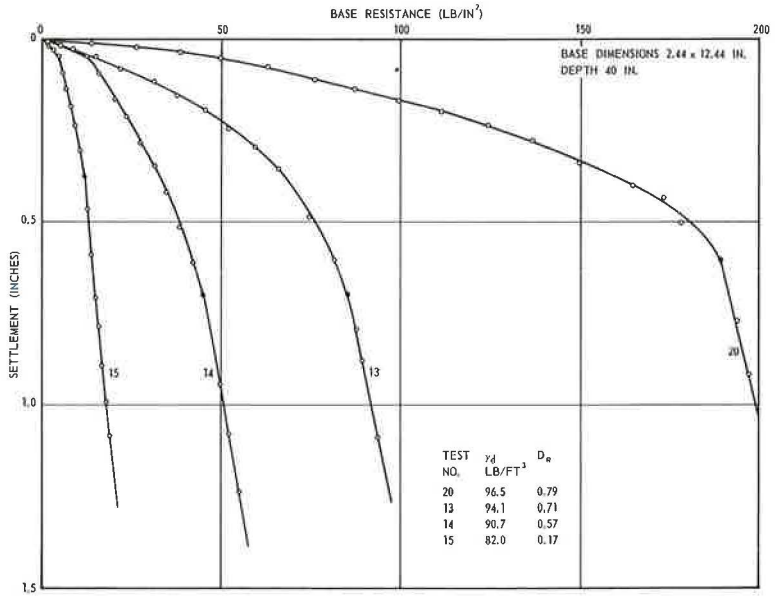

Figure 19. Typical results of base loading tests at greater depth.

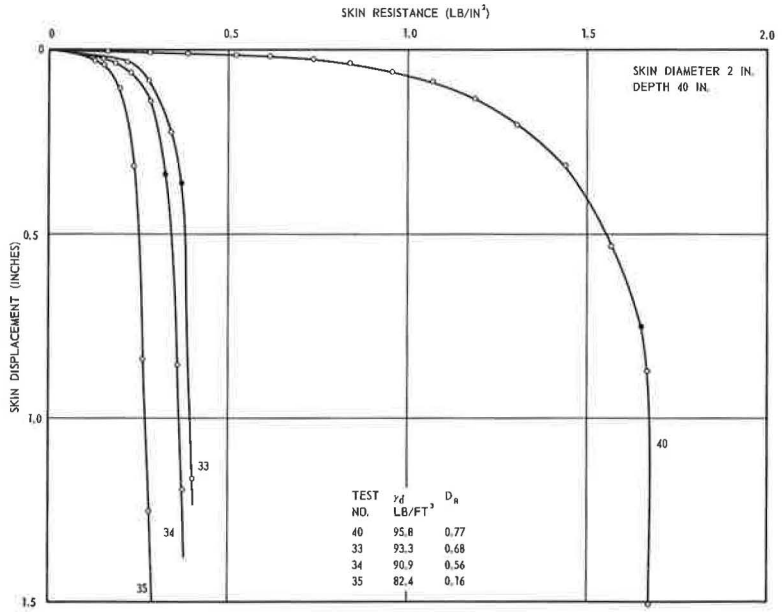

Figure 20. Typical results of skin loading tests.

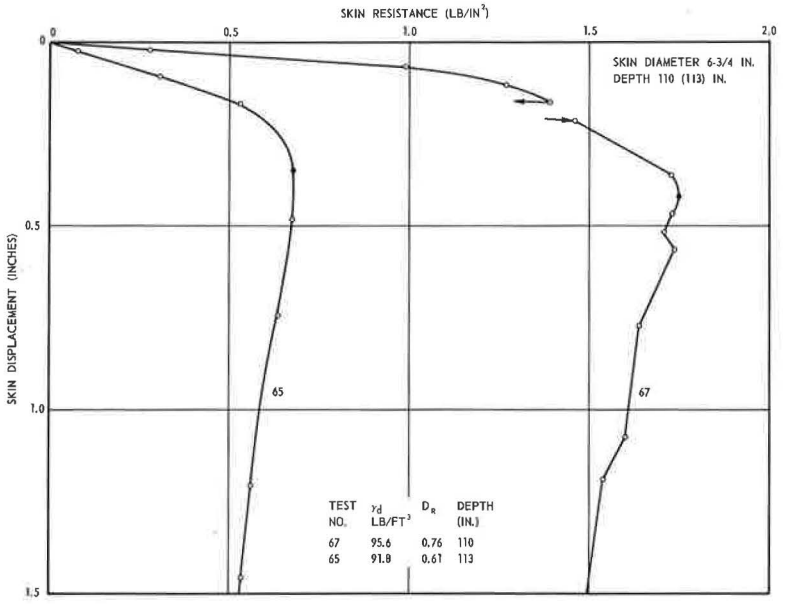

Figure 21. Typical results of skin loading tests.

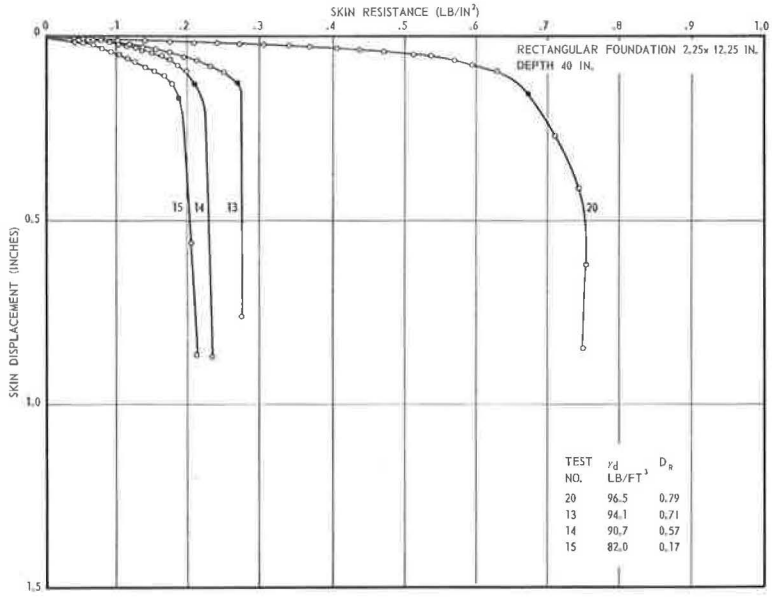

Figure 22. Typical results of skin loading tests.

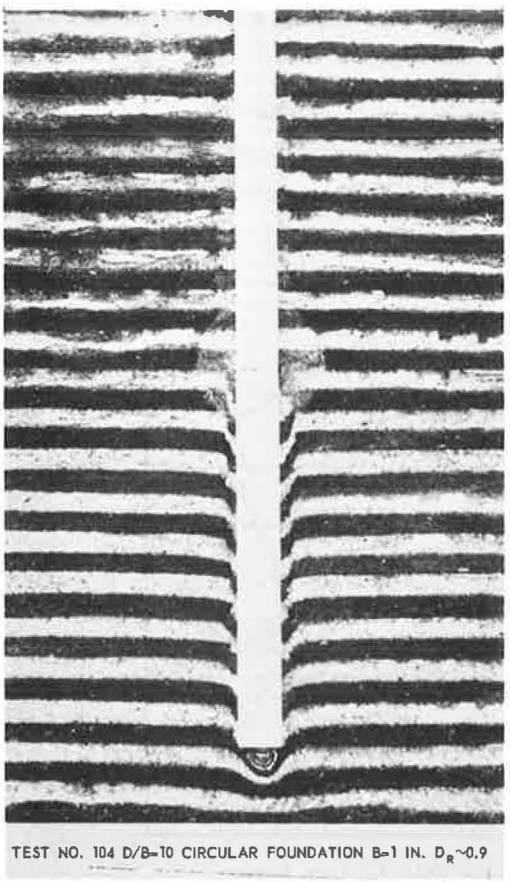

Figure 23. Shear pattern under a circular foundation placed at greater depth in very dense sand.

Figure 24. Shear pattern under a rectangular foundation placed at greater depth in very dense sand.

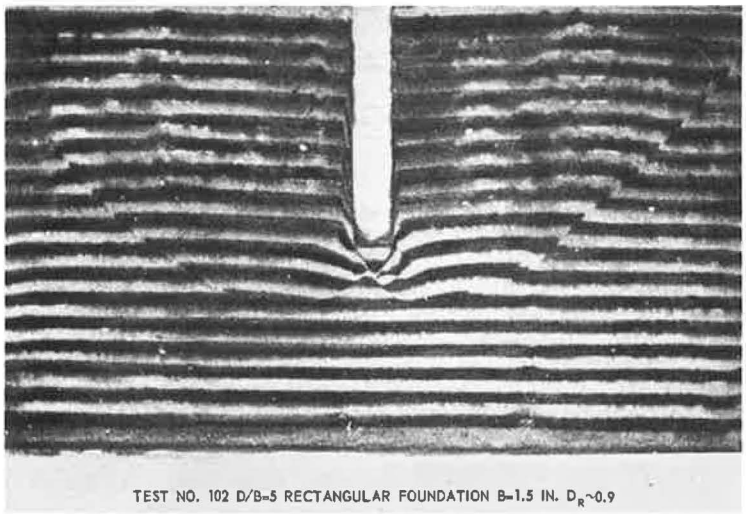

Figure 25. Shear pattern under a rectangular foundation placed at shallow depth in very dense sand.

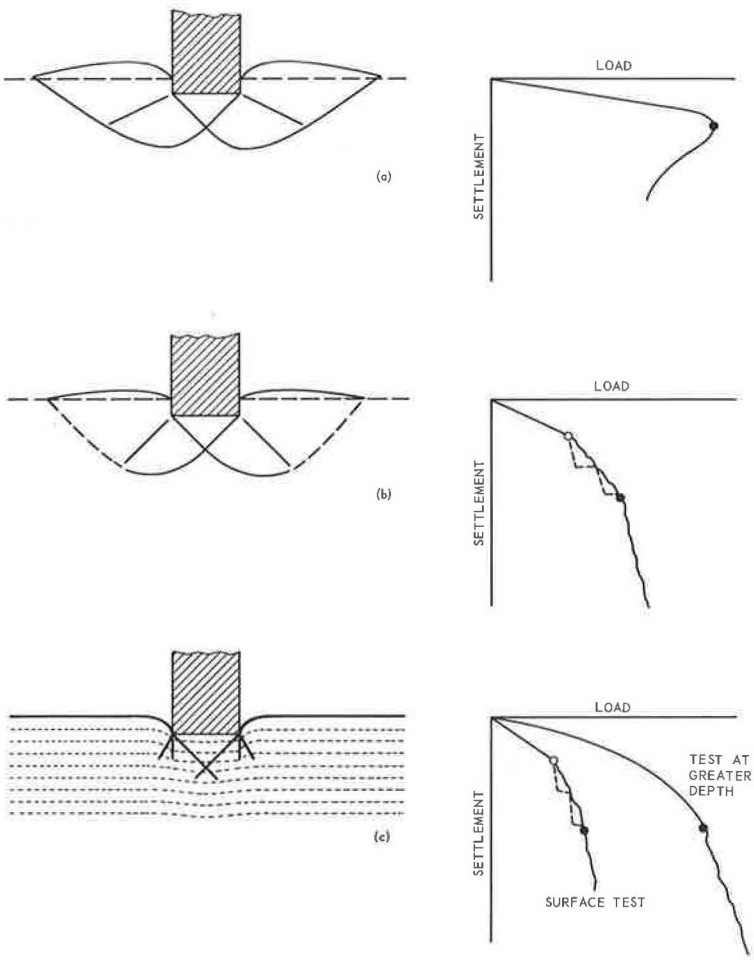

Figure 26. Types of failure.

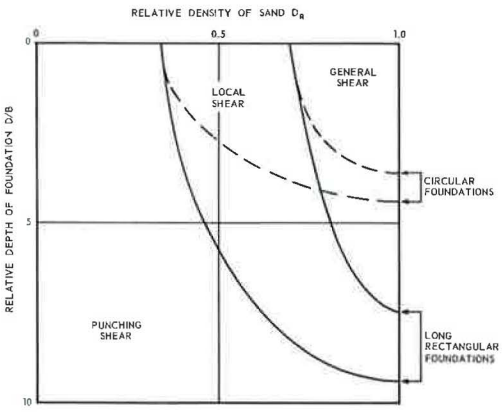

Figure 27. Types of failure at different relative depth D/B of foundations in sand.

Sudden shears can be observed in sequence as soon as the settlement reaches about 6 to 8 percent of foundation width. The failure surface, which is vertical or slightly inclined and follows the perimeter of the base, never reaches the sand surface. The phenomenon is essentially "punching shear failure," as described by De Beer and Vesić (34).

The same three characteristic types of failure are observed at shallow depths. However, as the relative depth D/B increases, the limiting relative densities at which failure types change increase. The approximate limits of types of failure to be expected as relative depth D/B and relative density of sand D_R vary are shown in Figure 27. There is a critical relative depth below which only punching shear failure occurs. For circular foundations this critical relative depth seems to be around D/B = 4, and for long rectangular foundations around D/B = 8.

It is important to note that the limits of types of failure depend on the compressibility of the material. More compressible materials will generally have lower critical relative depths. Following this trend, it is not difficult to explain why some materials may exhibit punching shear failure only.

Criterion of Failure or Ultimate Load

In accordance with observations just described the following criteria of failure or ultimate load were established:

1. In the case of general shear failure, the criterion is very clear: a peak of base resistance is always reached, corresponding to the appearance of failure surfaces at the sand surface, and to an abrupt change of rate of settlement from positive to negative.
2. In the case of local shear failure, there is not always a peak of base resistance, however, the rate of settlement reaches a maximum at the same load at which failure becomes visible at the surface. This load is considered as ultimate. In addition, first failure, clearly distinguishable only in stress-controlled tests, can be noted when settlements reach magnitudes at which the general shear failure occurs in dense sand (34).
3. In the case of punching shear failure, there is no peak of base resistance nor any appearance of failure surfaces. However, a peak of settlement rate can be noted. The corresponding load is considered as ultimate load.

Analogous criteria are adopted for skin loading tests.

DISCUSSION OF TEST RESULTS

Foundations at Surface

Figure 28 compares observed bearing capacities in surface tests with corresponding theoretical values. Measured values of $p/\frac{1}{2}\gamma B$ (col. 5, Tables 4 and 5) are shown as a function of dry unit weight of sand γ_d or relative density D_R. To have a better basis for comparison, the ultimate pressures of rectangular foundation have been multiplied by a shape factor 0.60 (a value recently confirmed by very extensive experiments, 35). Both first and ultimate failure pressures are shown for medium and loose sands. Figure 28 also shows theoretical bearing capacity factor N_γ after Caquot and Kerisel (36)

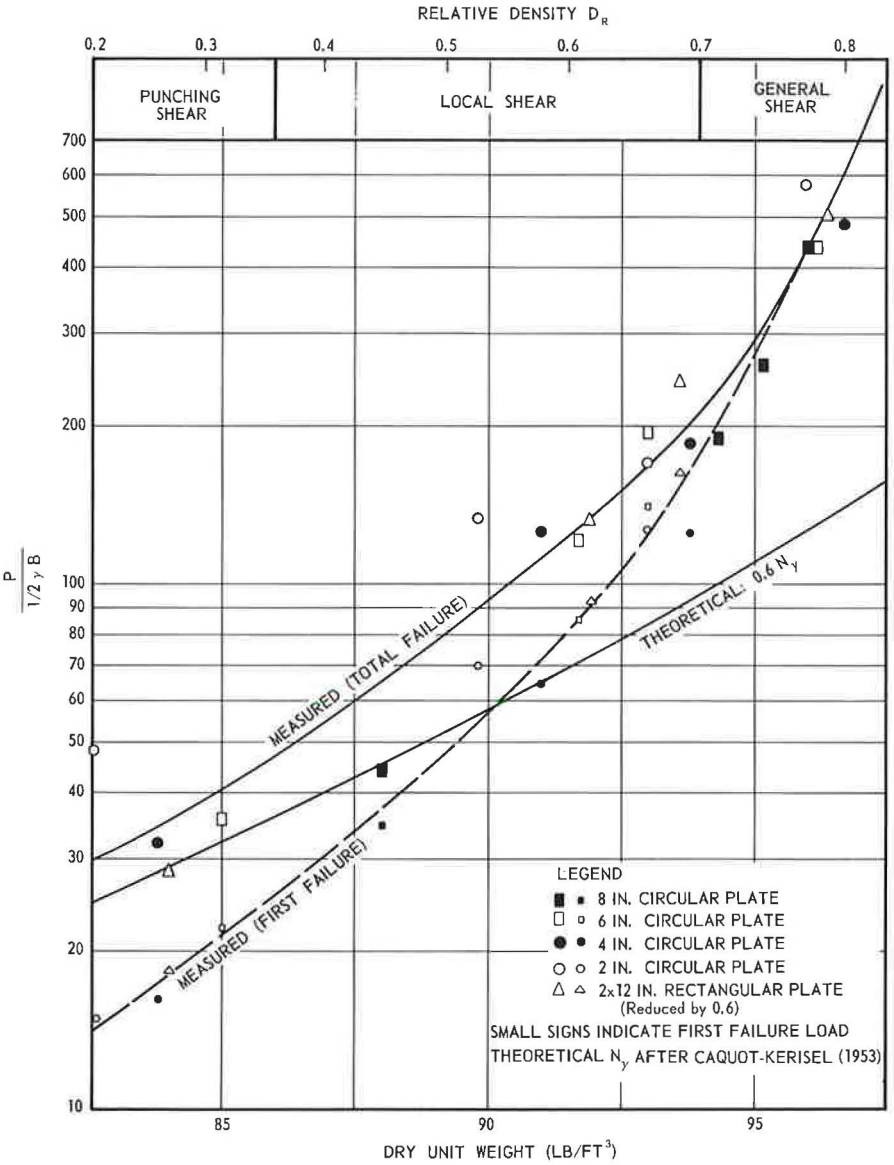

Figure 28. Observed bearing capacities of foundations at surface.

multiplied by shape factor 0.60. To present the factor N_γ as a function of dry unit weight or void ratio, the experimentally established relationship (Eq. 8) between the angle of internal friction ω and void ratio e is used.

Figure 28 shows that the observed ultimate bearing capacities are generally 1.2 to 4 times higher than corresponding theoretical values. This is in general agreement with findings of earlier experiments of similar nature (34, 33). A fully satisfactory explanation of this phenomenon has not yet been found.

The ranges of relative densities in which different types of failure occur (Fig. 28, top) also agree well with those found in an earlier investigation (34). It seems that the conventional classification of sands by relative density into loose ($D_R < 0.33$), medium ($0.33 < D_R < 0.67$) and dense ($D_R > 0.67$) has a certain meaning concerning the type of failure of shallow foundations on such materials.

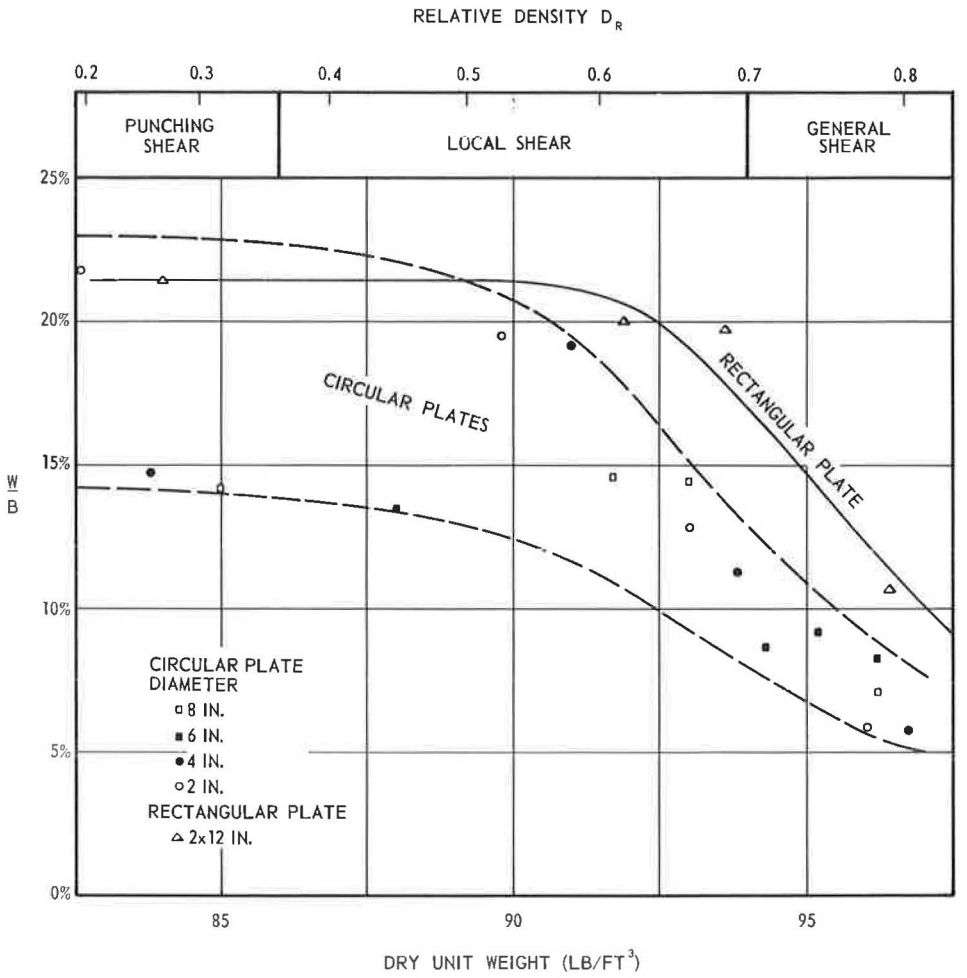

Figure 29. Settlement at failure for surface foundations.

Figure 29 shows the settlements at which ultimate loads were recorded, expressed as percentage of the foundation width. General shear failure usually occurs at settlements not exceeding 10 percent of foundation width; the other failure types take place at settlements of about 15 to 20 percent of the foundation width. This is in general agreement with former observations. However, slightly higher relative settlements at failure of rectangular foundations do not conform with some earlier findings (35). A similar trend was observed in tests with deep foundations (Fig. 32).

Base Resistance of Deep Foundations

Figures 30 and 31 show the general trend of increase in bearing capacity of the base with increase of foundation depth. Figure 30 shows the ultimate base resistance of 2.13-in. circular foundations as a function of foundation depth D. Figure 31 is an analogous plot for 2.44- by 12.44-in. rectangular foundations. A practically linear increase of bearing capacity with depth can be observed only at shallow depths, not exceeding approximately D/B = 4 for circular and D/B = 6 for rectangular foundations. As the foundation depth increases further, the rate of increase of bearing capacity with depth decreases. At a relative depth of approximately D/B = 15 the bearing capacity reaches asymptotically final values which appear to be functions of sand density only.

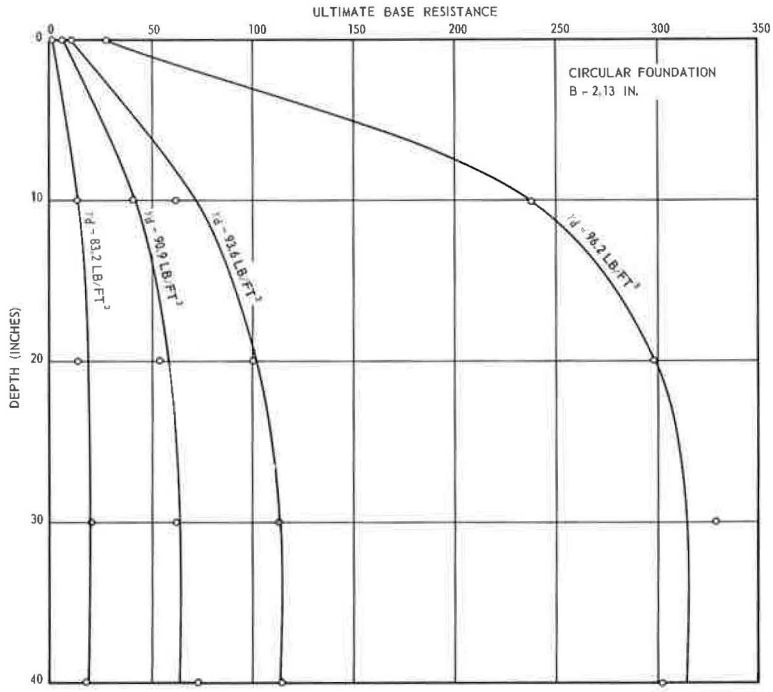

Figure 30. Measured bearing capacities of base—circular foundation, B = 2.13 in.

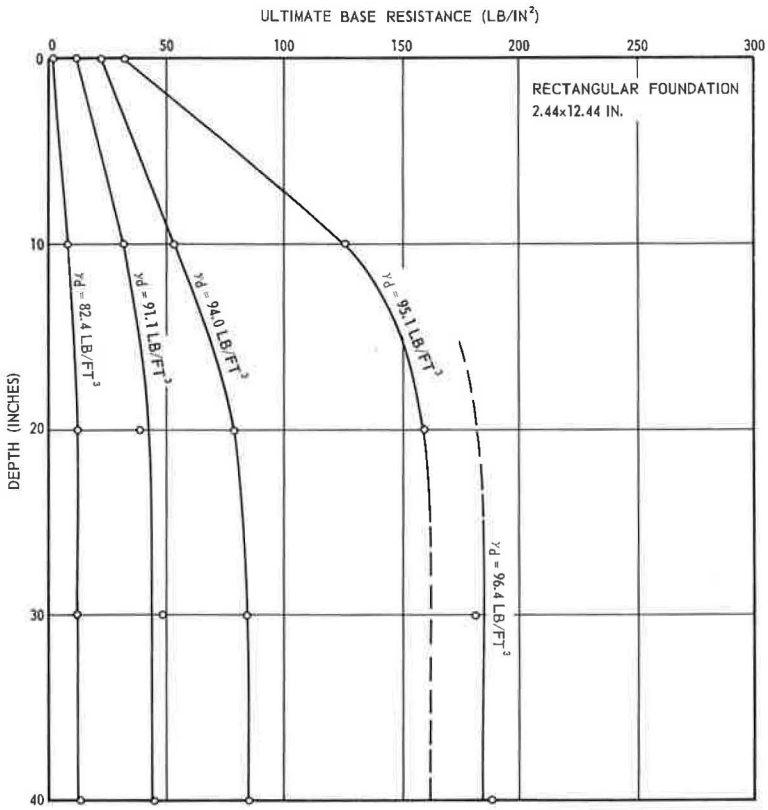

Figure 31. Measured bearing capacities of base—rectangular foundation, 2.44 x 12.44 in.

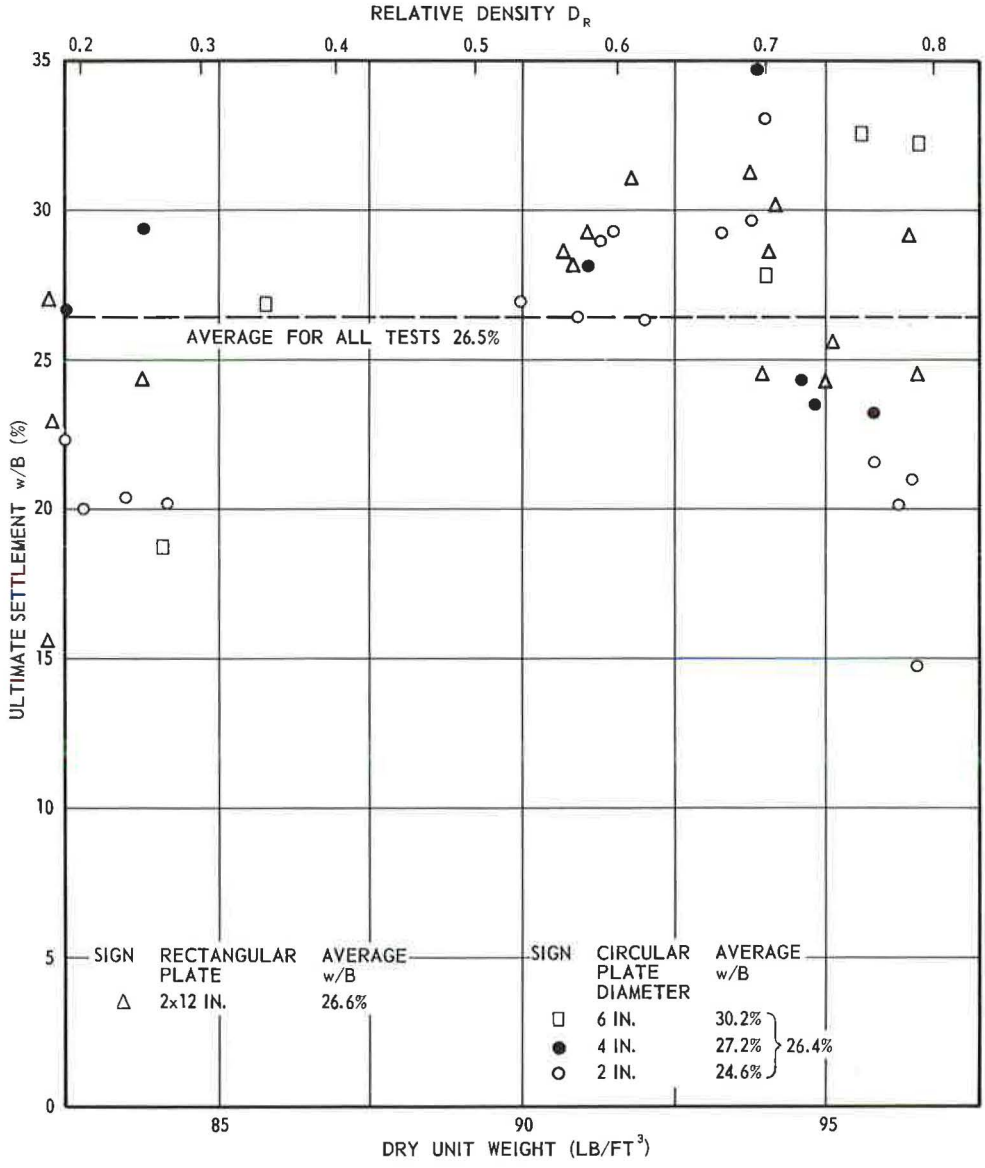

Figure 32. Ultimate settlement of deep foundations.

Base displacements or settlements needed to reach the ultimate loads are shown in Figure 32. Apparently, there is a tendency of ultimate settlements to increase with both foundation size and depth; however, this tendency is not pronounced. It may be stated that, in the range of foundations sizes and depth used in this investigation, ultimate loads are reached at settlements of about 20 to 30 percent of foundation depth. Figure 32 is in general agreement with isolated former observations.

A comparison of final bearing capacities of circular and long rectangular foundations indicates that the former are approximately 1.50 times higher. Figure 33 shows the average final bearing capacity of the base as a function of dry unit weight of sand, with bearing capacities of rectangular foundations multiplied by a shape factor of 1.50. Final bearing capacities observed in tests with 4- and 6.75-in. circular foundations are

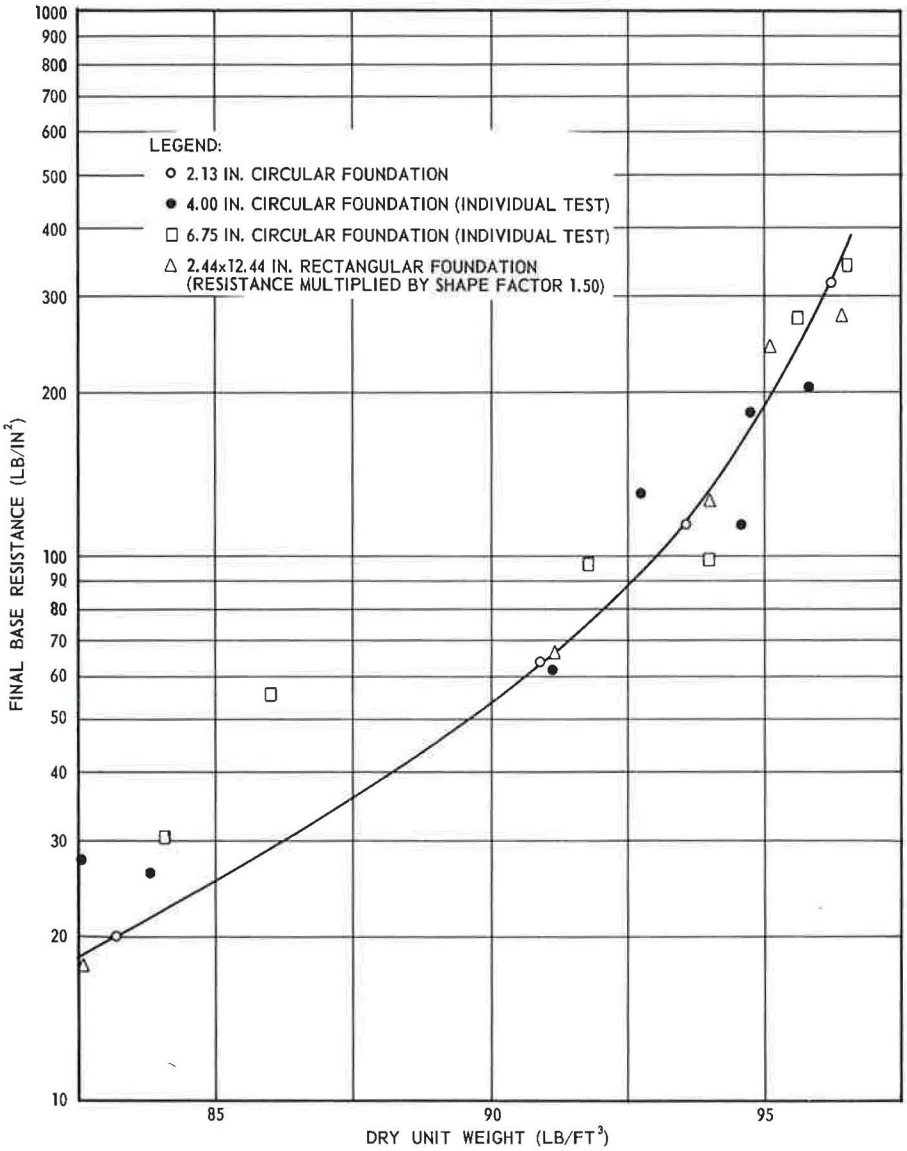

Figure 33. Ultimate base resistance at greater depth.

also plotted. The final bearing capacities are apparently independent of foundation size, at least for dense and medium dense sands.

A similar conclusion can be reached by studying Figure 6 of Kerisel's paper (32), although the numerical values obtained by the two investigations are not directly comparable due to differences in experimental approach and sand properties.

Skin Resistance of Deep Foundations

The variation of ultimate skin resistance s_0 with depth for 2-in. circular foundations is shown in Figure 34. For models in dense, vibrated sand, a long initial linear increase of s_0 with depth (up to D/B = 15) is followed by a sharp turn into a final skin resistance which remains constant as the depth increases further. For models in loose and medium-dense sand the shape of the initial part of the s_0 curve is not quite clear.

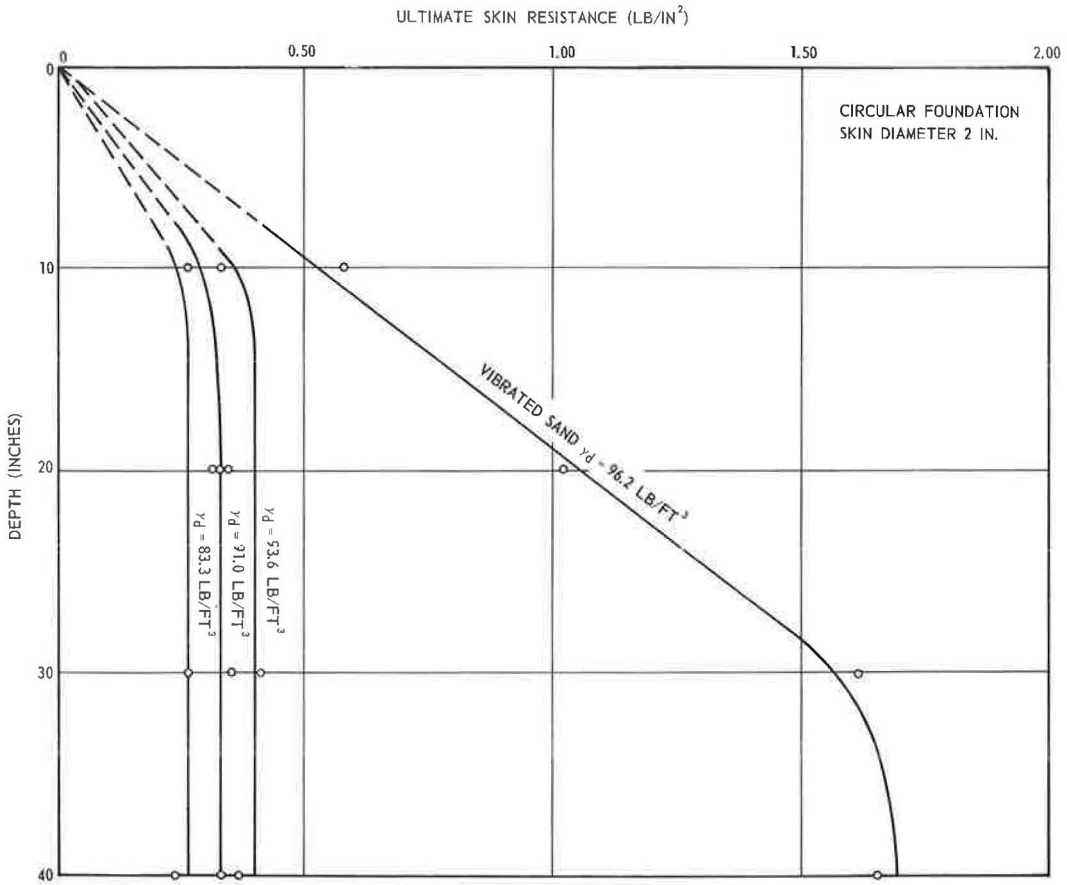

Figure 34. Ultimate skin resistance—circular foundation, 2 in.

It appears that there is also an initial linear increase limited to a depth of about four diameters. Beyond this depth the skin resistance turns sharply into a practically constant final value, varying with sand density only.

Figure 35 shows analogous diagrams for 2.25- by 12.25-in. rectangular foundations. The trend is similar, however, the initial part along which s_0 increases linearly with depth seems to be longer. The slope of the initial linear part is approximately three to four times less than the corresponding slope in the case of circular foundations. The final skin resistance, however, appears to be approximately 1.5 times lower for the rectangular shape.

Figure 36 shows the final average skin resistance as a function of dry unit weight of sand. Skin resistances of rectangular foundations multiplied by a shape factor of 1.5 are also plotted. The curve takes into account the fact that, due to method of placing of medium-dense sand, the density in the immediate vicinity of the skin was lower than the average density of the entire model, particularly in the case of 2-in. foundations.

The general shape of the s_0 curves found in the present investigation differs from that found in IRABA tests (32). However, it agrees well with numerous former observations on full-scale piers and caissons, which usually show a linear increase of s_0 at shallow depths, but a practically constant s_0 at greater depths.

Figure 37 shows skin displacements needed to reach ultimate skin resistance. It appears that these displacements are not dependent on foundation width and depth nor on sand density. For circular foundations they vary in the range of 0.30 to 0.40 in.; for rectangular foundations they are about one-half that magnitude. This finding con-

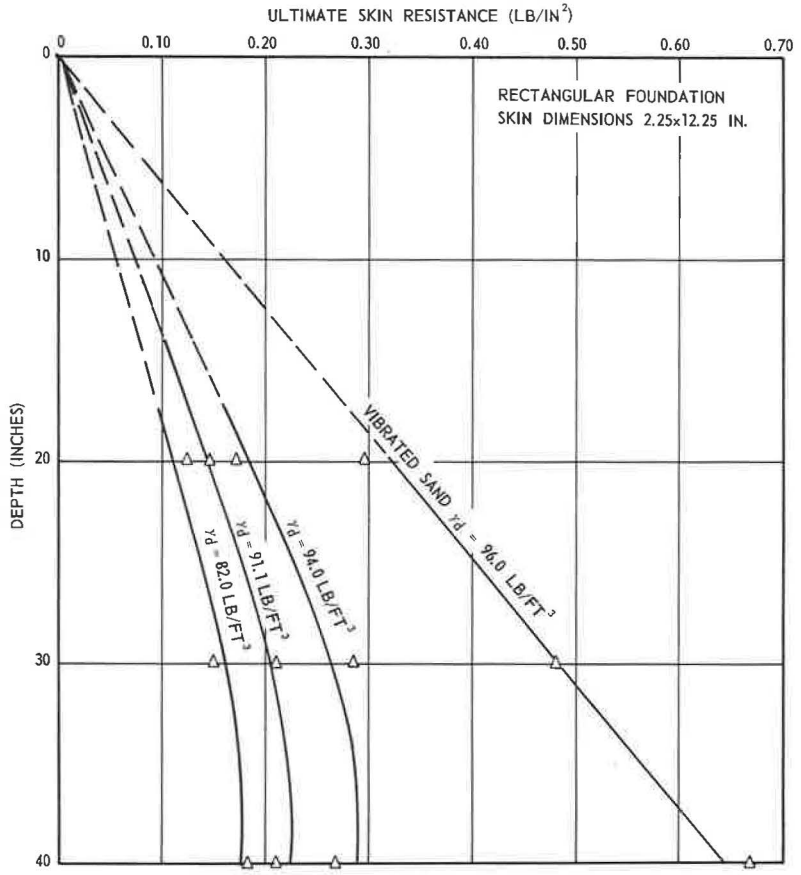

Figure 35. Ultimate skin resistance—rectangular foundation, 2.25 x 12.25 in.

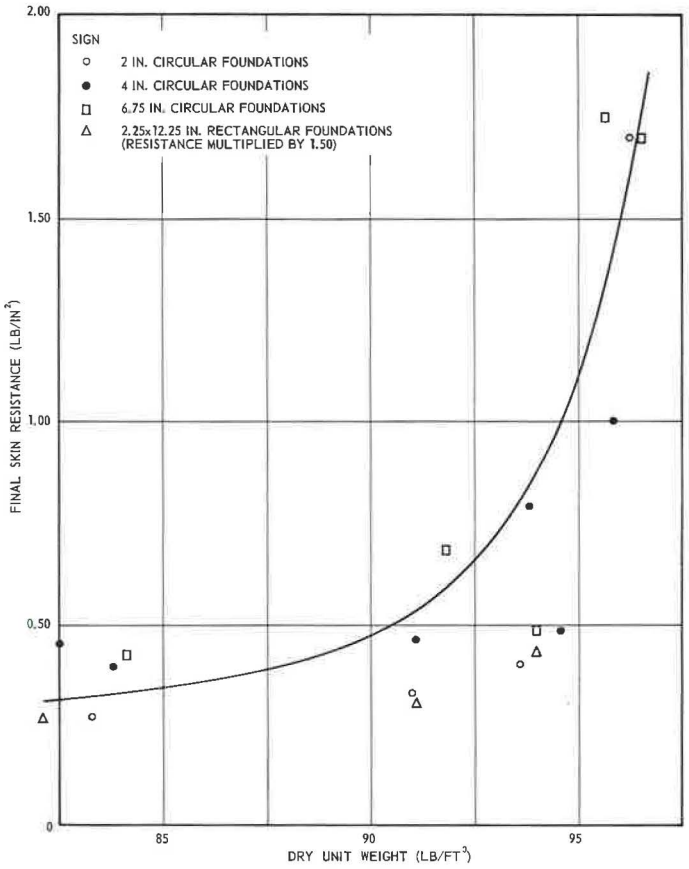

Figure 36. Final skin resistance at greater depth.

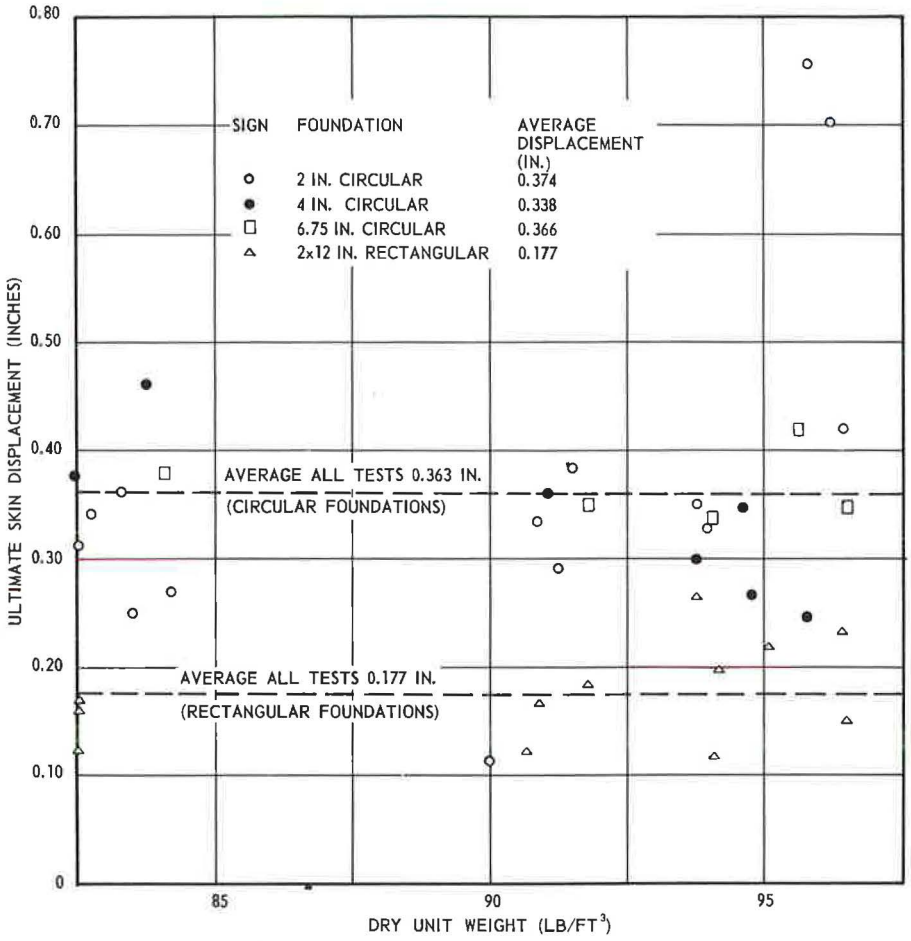

Figure 37. Ultimate skin displacement of deep foundations.

firms previously expressed beliefs that the mobilization of shear strength along a fixed rupture surface is governed by absolute displacement along that surface.

Bearing Capacity and Shape Factors at Shallow Depth

As previously mentioned, at shallow depths not exceeding D/B = 4 the increase of bearing capacity with depth appears to be linear as proposed by Eq. 3. Therefore the initial slopes of curves in Figures 30 and 31 indicate the experimental values of bearing capacity factor N_q at shallow depths. The N_q factors evaluated from these slopes are shown in Figure 38. To take into account the effect of shape, the depth term of circular foundations was reduced by an assumed shape factor of $\xi_q = 2.00$. Good agreement resulting from such an assumption indicates that shape factor ξ_q for a circular foundation in sand cannot differ greatly from 2. Terzaghi (6) proposed for that factor a value of 1.30 and Brinch Hansen (19), values increasing with φ from about 1.30 for $\varphi = 35°$ to 2.20 for $\varphi = 45°$.

As a basis for comparison, a curve of theoretical N_q values after Prandtl-Reissner is also shown (Fig. 38). To trace this curve the relationship (Eq. 8) between φ and e was assumed valid. This is justified by the probability that the average normal stress along a rupture surface under foundations does not exceed 10 percent of the foundation pressure.

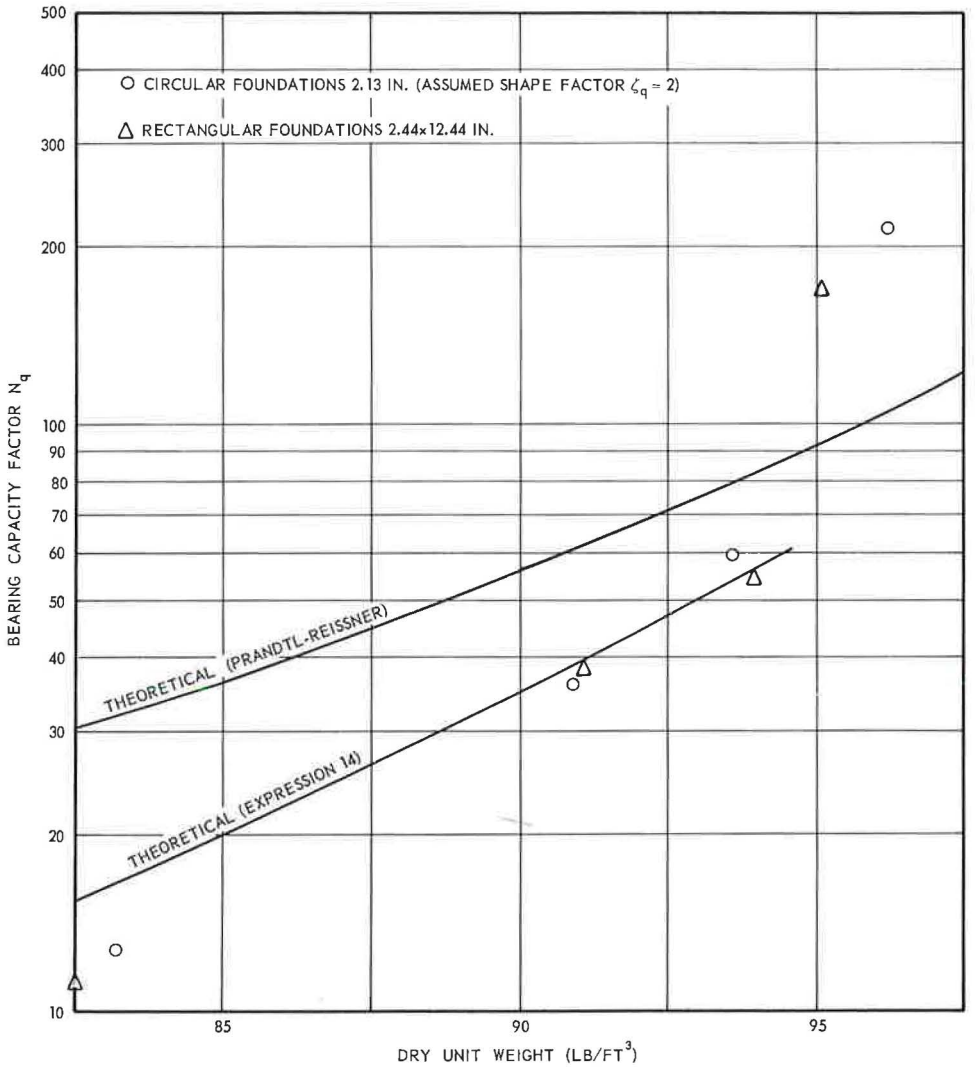

Figure 38. Measured bearing capacity factors N_q at shallow depth.

Higher N_q values for two very dense models can easily be explained. At high relative densities general shear failure still occurs at shallow depths (Figs. 25 and 27). As failure surfaces extend above foundation level, bearing capacity must be higher than indicated by Prandtl-Reissner theory which neglects shear resistance of the overburden (Fig. 2). If this resistance is taken into account a depth factor of approximately 2 should be introduced for D/B = 4 and $\varphi = 42°$ (10, 19). Therefore, excellent agreement of existing theory and experiments can be stated if the sand is dense. However, lower N_q values observed for medium and loose sand models cannot be explained by the existing theories, which consider general shear failure only.

Bearing Capacity in Local Shear Failure

To evaluate the bearing capacity factor N_q in the case of local or punching shear failure of a long rectangular foundation, a shear pattern based on observations on colored sand models will be considered (Fig. 39). It consists of an elastic zone ABC with two adjoining plastic zones BCD. The extent of development of these zones is determined by the angle θ at the apex.

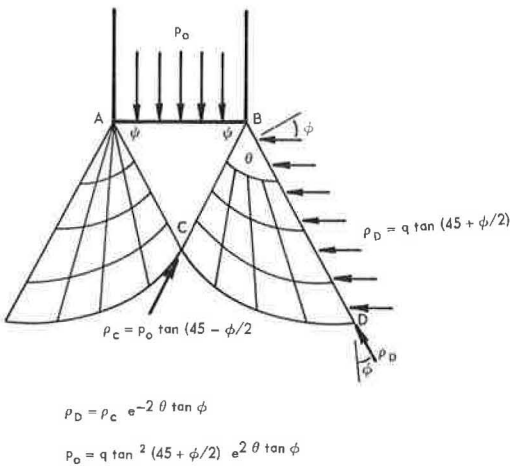

Figure 39. Analysis of punching or local shear failure.

It will be assumed that the overburden pressure q is great enough to allow neglecting the soil's own weight γ. Under such circumstances, solutions for weightless soil (3) can be applied to analyze stress conditions along CD. It is easy to show that the stress ρ_D acting on rupture line at D and the analogous stress ρ_C at C are connected by

$$\rho_D = \rho_C \, e^{-2\theta \tan \varphi} \tag{10}$$

However,

$$\rho_C = \rho_A = p_o \tan (45 - \varphi/2) \tag{11}$$

Also, assuming that the minor principal stress along BD is equal to overburden pressure q,

$$\rho_D = q \tan (45 + \varphi/2) \tag{12}$$

Eliminating ρ_C and ρ_D from Eqs. 10, 11, and 12,

$$p_o = q \tan^2 (45 + \varphi/2) \, e^{2\theta \tan \varphi} \tag{13}$$

By introducing $\theta = 1.9\,\varphi$, on the basis of observations, the following expression for N_q is obtained:

$$N_q = e^{3.8\,\varphi \tan \varphi} \tan^2 (45 + \varphi/2) \tag{14}$$

Numerical values for different angles φ are given in Table 10. They are lower than classical Prandtl-Reissner values. Reasonable agreement between N_q values computed by Eq. 14 and observed experimentally are shown in Figure 38.

Bearing Capacity at Greater Depth

Earlier discussion of base and skin resistances p_o and s_o has shown (Figs. 30 through 36) that, beyond some limiting relative depth D/B, the increase of p_o and s_o with depth is not linear. As D/B increases over 15, p_o and s_o do not increase any more. Final values of p_o and s_o appear to be functions of density of sand only (Figs. 33 and 36).

These observations seem to contradict the fundamental structure of bearing capacity Eq. 3 and 6 derived by using theories of plastic or elastic-plastic equilibrium. As previously mentioned, similar observations made recently by Kerisel (32) have led him to conclude that the bearing capacity factor N_q is a complex func-

TABLE 10

BEARING CAPACITY FACTOR N_q IN THE CASE OF LOCAL OR PUNCHING SHEAR FAILURE

Angle of Internal Friction, φ (deg)	Bearing Capacity Factor, N_q
0	1.0
5	1.2
10	1.6
15	2.2
20	3.3
25	5.3
30	9.5
35	18.7
40	42.5
45	115
50	422

tion of φ D/B and B. As long as no explanation of these findings is offered this appears to be the only possible conclusion.

However, attempts to explain the obtained results by an appropriate rational analysis leave serious doubts as to the correctness of the conclusion. No matter how limited an extent of plastic zone adjacent to the foundation base is assumed, there still must be a certain increase of p_o as overburden pressure increases. Therefore, N_q cannot be zero for any increment of loading as long as the same material is dealt with. When loosening of sand structure or significant crushing of sand grains occurs, there is still a lower limit of angle of internal friction of the newly formed material. Consequently, sooner or later, there must be an increase of p_o if overburden pressure continues to increase.

On the basis of these and other considerations, the conclusion was reached that constant values of p_o at greater depth do not result from decrease in N_q alone as suggested.

The explanation of the phenomena observed must, therefore, be sought through the assumption that q is not proportional to initial overburden pressure, as conventionally assumed. In connection with this, the true meaning of q in different theories should be remembered. In Prandtl-Reissner theory q is defined as normal stress at failure on horizontal plane of the foundation base (Fig. 2). In De Beer-Jaky-Meyerhof theories it is defined as normal stress at failure on the lower portion of the foundation shaft (Fig. 3). There is no good reason to take these stresses a priori equal or proportional to the initial overburden pressure, if foundation is deeply embedded in sand.

To demonstrate the meaning of the results, it is assumed that both p_o and s_o increase linearly with q as indicated by Eq. 3 and 6, but that q is strictly q_f or effective normal stress at failure acting on an elemental horizontal plane next to the foundation (Fig. 40). In a plane problem, or a rectangular foundation placed at greater depth, Eq. 3 can be rewritten in the following form:

$$p_o = q_f N_q \tag{15}$$

$$s_o = q_f K_s \tan \delta \tag{16}$$

Eliminating q_f

$$N_q = \frac{p_o}{s_o} K_s \tan \delta \tag{17}$$

In analogous way the following expressions can be written for a circular foundation:

$$p_o = q_f N_q \zeta_q \tag{18}$$

$$s_o = q_f K_s \tan \delta \zeta_s \tag{19}$$

$$N_q = \frac{p_o}{s_o} K_s \tan \delta \frac{\zeta_s}{\zeta_q} \tag{20}$$

Thus, it is possible to evaluate N_q from results of tests at greater depth under mentioned assumptions without really knowing q_f. $K_s \tan \delta$ or $K_s \tan \delta \zeta_s$ can be evaluated from the initial straight-line part of the s_o line.

The results of such an evaluation are shown in Figure 41, where individual results from tests at greater depth with 2- 4- and 6.75-in. circular foundations as well as with 2- by 12-in. rectangular foundations are plotted. To plot comparable magnitudes, both shape factors ζ_s and ζ_q for circular foundations were taken equal to 3 although ζ_s appeared to slightly higher. Figure 41 also shows, for comparison, bearing capacity factor N_q after Prandtl-Reissner and after Eq. 14. It is evident that experimental values obtained by using Eqs. 17 and 20 are primarily functions of sand density and that they are independent of absolute magnitude of q_f. Their numerical values in dense sand are reasonably well estimated by using the Prandtl-Reissner classical expression for N_q with a shape factor of approximately 3 for circular foundations. In medium and loose sands experimental values are lower, and comparable to those estimated by Eq. 14.

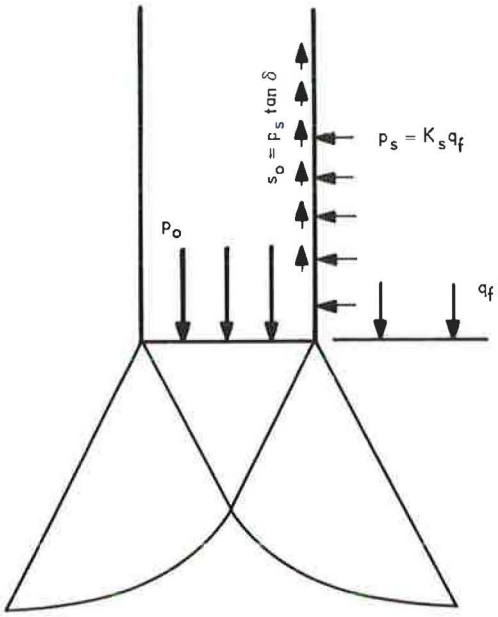

$$\frac{p_o}{q_f} = N_q = \frac{p_o}{s_o} K_s \tan \delta$$

Figure 40. Stress conditions in vicinity of base of deep foundation.

Some details of the analysis presented undoubtedly need further clarification, particularly the choice of shape factors which, due to limited number of tests performed, could not have been determined very accurately. It appears certain, however, that both base resistance p_o and skin resistance s_o are linear functions of vertical stress at failure, q_f. This stress is not necessarily equal nor proportional to the overburden pressure q. The nonlinear increase of base or skin resistance with depth can be explained by a similar increase of q_f with depth. If the base and skin resistance reach constant values at greater depth, it is because q_f also becomes constant at greater depth.

Analysis of Vertical Stress Around the Foundation

According to the preceding discussion, curves in Figures 30 and 31 indicate the nature of variation with depth of vertical stress at the base level, q_f. At shallow depths (D/B < 4), q_f is equal to the overburden stress q; at greater depths (D/B > 15), q_f reaches a constant value independent of overburden stress.

In a similar way, curves in Figures 34 and 35 indicate the variation of average vertical stress along foundation shaft q_s with foundation depth. From the shape of these curves it may be concluded that the distribution of vertical stresses q_z at any point z along the shaft must follow a curve similar to that in Figure 42c; namely, there should be a linear increase of q_z along a certain depth z_o, followed by a peak and gradual decrease to the final magnitude q_f. It is to be understood, however, that the foundation depth, sand density and some other factors may have influence on the shape of curves in question. Therefore, the peak mentioned may be more or less pronounced, or even nonexisting, leading to q_z curves of shapes between those in Figures 42c and 42b.

Looking for an explanation of this general trend of variation of q_z with depth, it was concluded that the nonlinear increase of bearing capacity with depth could be attributed to "arching" in sand above the foundation base. There exists, indeed, a striking similarity between curves in Figure 42 and curves of vertical pressure in a mass of sand above a yielding horizontal support (6, Fig. 18d).

On the basis of all the observations made, the following explanation of stress conditions around a deep foundation is suggested: When the foundation is loaded (Fig. 42a) the mass of sand beneath is compressed downward. At the same time sand around the foundation tends to follow the general downward movement of the mass. As a consequence of this, the originally horizontal stresses on a vertical plane n-n at a certain distance from the foundation become inclined. The inclination of these stresses is a function of the amount of displacement w of the foundation and of the distance z′ from the base level. If the foundation depth D is great enough, and if the base displacement w remains limited, there may be a distance z_o' beyond which the effect of downward movement is not felt any more. Above that distance stresses on vertical planes may remain horizontal, and the vertical stress q_z may be equal to overburden stress q.

The following arguments can be added in support of the explanation:

1. Measurements of displacements of sand surface during loading tests on foundations placed at greater depth (D/B > 8) showed downward movement of soil adjacent to the foundation.

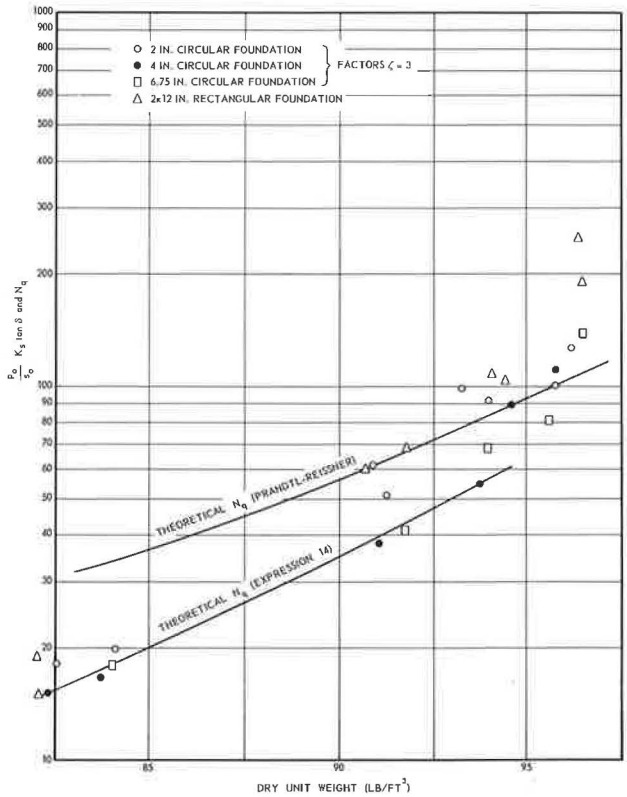

Figure 41. Bearing capacity factors at greater depth.

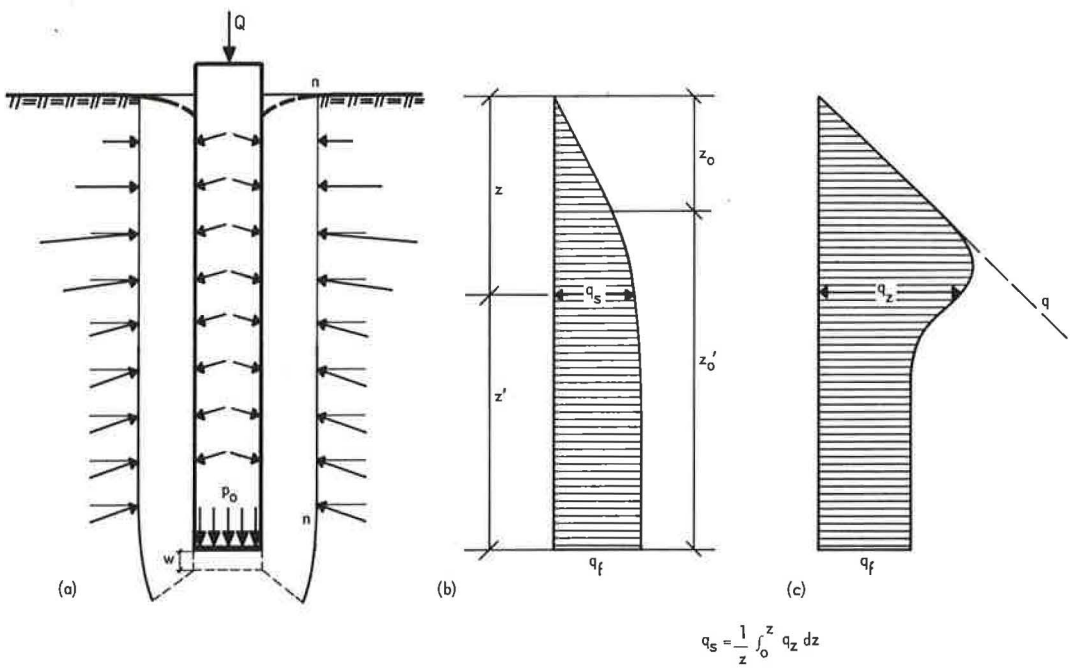

$$q_s = \frac{1}{z}\int_0^z q_z\, dz$$

Figure 42. Stress distribution around a deep foundation in sand.

2. Measurements of sand density around the foundation after load testing to failure indicated, in the case of models made of dense sand, considerable loosening in a zone immediately above base level, but a slight densification below that level.

3. Final resistances of the base and skin of rectangular foundations are found to be 1.50 times lower than corresponding resistances of circular foundations of the same diameter. However, measurements of real shape factor for base and skin resistances at greater depth indicate values of approximately 3. This leads to the conclusion that the final vertical stresses q_f around rectangular foundations are two times higher than corresponding stresses around circular foundations. The same ratio of final vertical stresses is found in the case of rectangular versus circular bins of the same diameter, where a similar phenomenon of arching occurs.

4. Under similar conditions there is less arching under smaller foundations, resulting in higher bearing capacity for the same relative depth D/B, because base displacements at failure increase proportionally to the foundation width. Displacement of a larger foundation will mobilize friction along relatively longer distance z_o.

5. Measurements of skin resistance along model foundations in sand have indicated distributions similar to curves in Figure 42 (38, 39).

Numerous other observations on actual deep foundations as well as on models can be cited in favor of the explanation offered. However, it should be realized that the problem in question is very complex, and that variables such as roughness of foundation skin or method of construction may also be of significant influence.

A special study of this problem, including the development of a method for rational analysis of stresses around deep foundations in a homogeneous sand stratum is in progress.

CONCLUSIONS

1. Shear patterns observed underneath buried model foundations in sand indicate that, depending on relative density of sand, all three types of failure previously described in the literature may occur at shallow depth: general shear failure, local shear failure and punching shear failure. However, at greater depths only punching shear failure occurs, irrespective of relative density of sand. Limits of types of failure to be expected vary with relative density or compressibility as well as with relative depth D/B of the foundation (Fig. 27).

2. At shallow depths, not exceeding four foundation widths ($D/B < 4$) the increase of point bearing capacity with depth is linear. In dense sand ($D_R > 0.70$) the bearing capacity factor N_q can be estimated with sufficient accuracy using an analysis based on conventional theory of general shear failure in a rigid-plastic solid. In loose or medium-dense sand, failure surfaces being localized, better agreement with test results may be stated if an expression for N_q derived under the assumption of local or punching shear failure is used.

3. At greater depths, generally exceeding 15 foundation widths, both base resistance p_o and skin resistance s_o reach constant final values. These values are independent of overburden pressure q and appear to be functions of relative density of sand only. This is explained by the arching of sand above the foundation base. It is demonstrated that both p_o and s_o are proportional to the effective vertical stress at failure, q_f at the level of foundation base.

4. The bearing capacity factory N_q at greater depth, defined as the ratio of base resistance p_o to vertical stress q_f, is practically independent of foundation size and is a function of relative density or angle of internal friction of sand. Observed bearing capacity factors N_q for long rectangular foundations at greater depth do not differ from those at shallow depth. However, the shape factor for circular foundations appears to be somewhat higher at greater depths.

5. Skin resistance along the foundation shaft is not necessarily increasing linearly with depth. Instead, it is proportional to the vertical stress q_z at the corresponding elevation. Vertical stress increases linearly only at shallow depths. If the foundation is deeply embedded in sand, the distribution of vertical stress, as well as of skin resistance, is likely to be similar to that in Figure 42.

6. The fundamental fallacy of conventional analyses of bearing capacity of deep foundations in sand consists in the assumption that q is always equal to the initial overburden stress at the level of foundation base. This may be correct if a deep foundation penetrates only slightly into a sand stratum overlain by compressible soil. However, it may be entirely wrong if a deep foundation is completely embedded in sand.

ACKNOWLEDGMENTS

The tests described in this paper have been performed in the Soil Mechanics Laboratory of Georgia Institute of Technology, Atlanta, Georgia. The investigation is being sponsored by the State Highway Department of Georgia and the U. S. Bureau of Public Roads. Thanks are due to officials of these institutions for their interest and support. The pile testing area has been constructed and equipped using funds allocated by the Engineering Experiment Station, Georgia Institute of Technology. The contributions of McKinney Drilling Company and Armco Drainage & Metal Products, Inc., are gratefully acknowledged.

The author is indebted to James M. Duncan, Don C. Banks, and Ray L. Holmes, Graduate Research Assistants, who assisted in construction of equipment and performed the loading tests. Special credit is due to Guillermo Restrepo, Graduate Student, for preparation and testing of two models with colored sand. Graduate Research Assistants, O. S. Lord, R. C. Williams, and W. L. Boyd, as well as Student Assistants, T. W. Russell, D. E. Hodges, and Houshang Rahimzadeh, also gave much valuable help in different phases of the project.

Finally, the author wishes to express his thanks to Robert E. Stiemke, Director of the Engineering Experiment Station, for his help and encouragement in the early stages of the project. He is also grateful to Mrs. Milena A. Sedmak Vesić for her interest and assistance in preparation of diagrams.

REFERENCES

1. Prandtl, L., "Uber die Harte plastisher Korper." Nachrichten Kon. Gesell. der Wissenschaffen, Math. Phys. Klasse, 74-85, Gottingen (1920).
2. Prandtl, L., "Uber die Eindringungsfestigkeit plastisher Baustoffe und die Festigkeit von Schneiden." Zeitschrift fur Angewandte Mathematik und Mechanik, 1: 1, 15-20 (1921).
3. Reissner, H., "Zum Erddruckproblem." Proc. First Intern. Conf. Applied Mech., 295-311, Delft (1924).
4. Caquot, A., "Equilibre des massifs a frottement interne." Gauthier-Villars, Paris (1934).
5. Buisman, A. S. K., "De weerstand van paalpunten in zand." De Ingenieur, 50: 25-28, 31-35 (1935).
6. Terzaghi, K., "Theoretical Soil Mechanics." Wiley (1943).
7. De Beer, E. E., "Donnees concernant la resistance au cisaillement deduites des essais de penetration en profondeur." Geotechnique, 1: 22-40 (1948).
8. De Beer, E. E., " Etude des fondations sur pilotis et des fondations directes." Annales des Travaux Publics de Belgique, 46: 1-78 (1945).
9. Jaky, J., "On the Bearing Capacity of Piles." Proc., Sec. Intern. Conf. Soil Mech. and Found. Engg., 1: 100-103, Rotterdam (1948).
10. Meyerhof, G. G., "The Ultimate Bearing Capacity of Foundations." Geotechnique, 2: 301-332 (1951).
11. Meyerhof, G. G., "Recherches sur la force portante des pieux." Annales de l' Institut Technique du Batiment et des Travaux Publics, 6: 63-64, 371-374 (1953).
12. Berezantsev, V. G., "Osesimetrichnaia zadacha teorii predel 'nogo ravnovesia sypuchei sredy." Gostechizdat, Moscow (1952).
13. Bishop, R. F., Hill, R., and Mott, N. F., "The Theory of Indentation and Hardness Test." Proc. of the Physical Soc., 57: 147-159 (1945).
14. Gibson, R. E., Discussion. Jour. Instit. of Civil Engineers, 34: 382 (1950).

15. Skempton, A. W., Yassin, A. A., and Gibson, R. E., "Theorie de la force portante des pieux." Annales de l'Institut Rechnique du Batiment et des Travaux Publics, 6: 63-64, 285-290 (1953).
16. Ladanyi, B., "Etude theorique et experimentale de l'expansion dans un sol pulverulent d'une cavite presentant une symetrie spherique ou cylindrique." Annales des Travaux Publics de Belgique, 62: 105-148, 365-406 (1961).
17. Brinch Hansen, J., "Simple Statical Computation of Permissible Pile Loads." Christiani and Nielsen Post, 14-17 (1951).
18. Caquot, A., and Kerisel, J., "Traite de Mecanique des Sols." 3rd edit. Gauthier-Villars, Paris (1956).
19. Brinch Hansen, J., "A General Formula for Bearing Capacity." Danish Technical Institute, Bull. 11, Copenhagen (1961).
20. Delft Soil Mechanics Laboratory, "The Predetermination of the Required Length and the Prediction of the Toe Resistance of Piles." Proc. Intern. Conf. on Soil Mech. and Found. Engg., I: 181-184, Cambridge, Mass. (1936).
21. Plantema, G., "Results of a Special Loading Test on a Reinforced Concrete Pile." Proc. Sec. Intern. Conf. Soil Mech. Found. Engg., IV: 112-118, Rotterdam (1948).
22. Huizinga, T. K., "Application of Results of Deep Penetration Tests to Foundation Piles." Building Research Congress, 173-179, London (1951).
23. Van der Veen, C., "The Bearing Capacity of a Pile." Proc. Third Int. Conf. Soil Mech. Found. Engg., II: 84-90, Zurich (1953).
24. Van der Veen, C., and Boersma, L., "The Bearing Capacity of a Pile Predetermined by a Cone Penetration Test." Proc. Fourth Intern. Confer. on Soil Mech. and Found. Engg., II: 76-78, London (1957).
25. Bogdanovic, Lj., "The Use of Penetration Tests for Determining the Bearing Capacity of Piles." Proc. Fifth Intern. Confer. Soil Mech. Found. Engg., II: 17-22, Paris (1961).
26. Geuze, E. C. W. A., "Resultats d'essais de penetration en profondeur et de mise en charge de pieux." Annales de l'Institut Technique du Batiment et des Travaux Publics 6: 63-64, 313-319 (1953).
27. De Beer, E. E., "Les essais de penetration en profondeur." Unpublished lecture, Yugoslavia (1955).
28. Kahl, H. and Muhs, H., "Uber die Untersuchung des Baugrundes mit einer Spitzendrucksonde." Die Bautechnik, 29: 81-88 (1952).
29. Kerisel, J., "Deformations et contraintes au voisinage des pieux." Bull. 10, A. B. E. M., Brussels (1953).
30. L'Herminier, R., "Remarques sur le poinconnement continu des sables et graviers." Annales de l'Institut Technique du Batiment et des Travaux Publics, 6: 63-64, 371-374 (1953).
31. Berezantsev, V. G., "Raschet prochnosti osnovania sooruzhenii." Gosstroiizdat, Ch. III, Moscow (1960).
32. Kerisel, J., "Foundations profondes en milieu sableux." Proc., Fifth Intern. Confer. Soil Mech. Found. Engg., II: 73-83, Paris (1961).
33. Hansen, Bent, and Odgaard, D., "Bearing Capacity Tests on Circular Plates on Sand." Danish Technical Institute, Bull. 8, 19 pp., Copenhagen (1960).
34. De Beer, E. E., and Vesić, A. B., "Etude experimentale de la capacite portante du sable sous des foundations directes etablies en surface." Annales des Travaux Publics de Belgique, 59: 3, 5-58 (1958).
35. De Beer, E. E., and Ladanyi, B., "Etude Experimentale de la capacite portante du sable sous des fondations circulaires etablies en surface." Proc. Fifth Intern. Confer. Soil Mech. Found. Engg., I: 577-585, Paris (1961).
36. Caquot, A., and Kerisel, J., "Sur le terme de surface dans le calcul des fondations en milieu pulverulent." Proc. Third Intern. Confer. Soil Mech. Found. Engg., I: 336-337, Zurich (1953).
37. L'Herminier, R., Habib, P., Tcheng, Y., and Bernede, J., "Fondations superficielles." Proc. Fifth Intern. Confer. Soil Mech. Found. Engg., I: 713-717, Paris (1961).

38. Zweck, H., "Mesures sur modeles reduits du frottement lateral et de la resistance de pointe des pieux." Annales de l'Institut Technique du Batiment et des Travaux Publics, 6: 63-64, 367-370 (1953).
39. Habib, P., "Essais de charge portante de pieux en modele reduit." Annales de l'Institut Technique du Batiment et des Travaux Publics, 6: 63-64, 361-366 (1953).